



**HAL**  
open science

## Use of A-train satellite observations (CALIPSO-PARASOL) to evaluate tropical cloud properties in the LMDZ5 GCM

D. Konsta, J.-L D Dufresne, H Chepfer, A Idelkadi, G Cesana

► **To cite this version:**

D. Konsta, J.-L D Dufresne, H Chepfer, A Idelkadi, G Cesana. Use of A-train satellite observations (CALIPSO-PARASOL) to evaluate tropical cloud properties in the LMDZ5 GCM. *Climate Dynamics*, 2016, 47 (3), pp.1263-1284. 10.1007/s00382-015-2900-y . hal-01384436

**HAL Id: hal-01384436**

**<https://hal.science/hal-01384436>**

Submitted on 19 Oct 2016

**HAL** is a multi-disciplinary open access archive for the deposit and dissemination of scientific research documents, whether they are published or not. The documents may come from teaching and research institutions in France or abroad, or from public or private research centers.

L'archive ouverte pluridisciplinaire **HAL**, est destinée au dépôt et à la diffusion de documents scientifiques de niveau recherche, publiés ou non, émanant des établissements d'enseignement et de recherche français ou étrangers, des laboratoires publics ou privés.

1

**Use of A-train satellite observations (CALIPSO-PARASOL) to evaluate tropical cloud properties in the LMDZ5**

**GCM**

D. Konsta, J.-L. Dufresne, H. Chepfer, A. Idelkadi, G.Cesana

Laboratoire de Météorologie Dynamique (LMD/IPSL), Paris, France

LMD/IPSL, UMR 8539, CNRS, Ecole Normale Supérieure, Université Pierre et Marie Curie, Ecole Polytechnique

2

3

4

5

## 6 **Abstract**

7 The evaluation of key cloud properties such as cloud cover, vertical profile and optical depth as well as the analysis of their  
8 intercorrelation lead to greater confidence in climate change projections. In addition, the use of collocated and instantaneous  
9 data facilitates the links between observations and parameterizations of clouds in climate models.

10 New space-borne multi-instruments observations collected with the A-train make simultaneous and independent  
11 observations of the cloud cover and its three-dimensional structure at high spatial and temporal resolutions possible. The  
12 CALIPSO cloud cover and vertical structure and the PARASOL visible directional reflectance, which is a surrogate for the  
13 cloud optical depth, are used to evaluate the representation of cloudiness in two versions of the atmospheric component of  
14 the IPSL-CM5 climate model, LMDZ5 GCM. A model to satellite approach in applying the CFMIP Observation Simulation  
15 Package (COSP) is used to allow a quantitative comparison between model results and observations.

16 The representation of clouds in the two model versions is first evaluated using monthly mean data. This classical approach  
17 reveals model biases of different magnitudes depending on the model version used. These biases are an underestimation of  
18 cloud cover associated to an overestimation of cloud optical depth, an underestimation of low- and mid-level tropical clouds  
19 and an overestimation of high clouds. The difference between models of these biases clearly highlights the improvement of  
20 the amount of boundary layer clouds, the improvement of the properties of high-level clouds and the improvement in  
21 simulating mid-level clouds in the tropics thanks to the new convective, boundary layer, and cloud parameterizations  
22 included in LMDZ5B compared to the previous LMDZ5A version. The correlation between instantaneous cloud properties  
23 allows for a process-oriented evaluation for tropical oceanic clouds. This evaluation shows that the cloud population with  
24 intermediate values of cloud cover and cloud reflectance when using monthly mean is now split in two groups of clouds,  
25 one with low and intermediate values of the cloud cover and another one with cloud cover close to one. The precise  
26 determination of cloud height allows us to focus on specific types of clouds (i.e. boundary layer clouds, high clouds, low-  
27 level clouds with no clouds above). For low-level clouds over the tropical oceans, the correlation between instantaneous  
28 values of the cloud cover and cloud reflectance reveals a major bias in the simulated liquid water content for both model  
29 versions. The origin of this problem is determined and possible improvements such as considering the sub-grid  
30 heterogeneity of cloud properties are investigated using sensitivity tests. In summary, the analysis of the relationship  
31 between different instantaneous and collocated variables allows for process-oriented evaluations. These in turn may help to  
32 improve model parameterizations and may also help to bridge the gap between model evaluation and model development.

33 **1. Introduction**

34

35 The evaluation of clouds simulated by general circulation models (GCMs) generally relies on monthly mean values [e.g. Yu  
36 et al., 1996, Webb et al. 2001, Zhang et al. 2005], which do not contain detailed information on the transient aspects of  
37 cloud behavior. Using monthly mean values might lead to a quantitative way to calibrate models in order to match present-  
38 day observations with present-day simulations but these monthly means lack details on the cloud processes that create them.  
39

40 The A-train jointly observes the cloud radiative properties using the passive remote sensors PARASOL (Polarization &  
41 Anisotropy of Reflectances for Atmospheric Sciences coupled with Observations from a Lidar) [e.g. Parol et al. , 2004] and  
42 CERES (Clouds and the Earth's Radiant Energy System) [Wielicki et al., 1996] as well as the cloud vertical structure using  
43 the new generation of satellites carrying lidar instruments CALIOP/CALIPSO (Cloud-Aerosol Lidar and Infra-red  
44 Pathfinder Satellite Observations) [Winker et al. 2007]. This joint observation dataset constitutes a unique opportunity to  
45 perform quantitative evaluations of GCM cloudiness [Chepfer et al., 2008, Marchand et al., 2009, Zhang et al., 2010,  
46 Cesana and Chepfer, 2013]. The ability of the A-train to simultaneously observe the radiative properties of clouds and their  
47 three-dimensional distribution at the instantaneous time scale (typically on the order of tens of seconds) and at high spatial  
48 resolution [Konsta et al., 2012] is used to provide new observational constraints to evaluate the representation of cloud  
49 processes in climate models.

50

51 A major aim of physical parameterizations in GCMs is to reproduce the mean properties of cloud variables as well as the  
52 relationships between these cloud variables and the dynamic and thermodynamic state of the atmosphere. If models fail to  
53 reproduce these key features, they may lack the ability to properly predict cloud variations under environmental changes,  
54 cloud feedbacks and the cloud response to anthropogenic forcing. A key step is thus to evaluate the mean properties of  
55 clouds and to evaluate how they vary in response to a change of the physical characteristics of their environment. The  
56 instantaneous analysis of cloud properties facilitates a direct relationship between observations and model  
57 parameterizations. Some meteorological features occur at instantaneous time scale but are lacking when using monthly  
58 mean values, such as the complex multi-layer structure of mesoscale convective systems or the inhomogeneous spatial  
59 structure of marine stratocumulus. These features have an important impact on the radiative effect of clouds and therefore  
60 on the magnitude of cloud feedbacks as the two are strongly correlated [Brient and Bony, 2012].

61

62 Short time scales may be considered during the development stage of a model. For instance, some recent developments in

63 the LMDZ atmospheric model have been undertaken in order to improve the diurnal cycle of precipitation and to solve the  
64 long-standing problem of too early precipitations in tropical regions [Rio et al., 2013]. The following questions are  
65 addressed:

66 1) Have the recent developments in the LMDZ5B atmospheric model improved the representation of clouds' physical  
67 properties?

68 2) Can the instantaneous spatial observations allow for the identification of remaining problems in the model representation  
69 of clouds? and

70 3) What role plays the cloud heterogeneities at the model's subgrid scale for the remaining problems in representing cloud in  
71 models?

72 The simulated cloud occurrence, vertical structure and optical depth of tropical oceanic clouds are compared with A-train  
73 observations. Monthly mean values are first considered as it is the common time scale used in climate model evaluation.  
74 Instantaneous values are then used to facilitate the interpretation of results in term of model parameterization because the  
75 statistical relationships between cloud variables at these two time scales have been shown to be significantly different  
76 [Konsta et al., 2012]. Observations provided by CERES are used to evaluate the cloud shortwave radiative albedo,  
77 observations provided by PARASOL are used to evaluate the cloud optical depth, and observations provided by  
78 CALIOP/CALIPSO are used to evaluate the cloud cover and the cloud vertical profile.

79  
80 The two versions of the LMDZ5 atmospheric model, the A-train observations and the observations simulators are briefly  
81 described in Section 2. The cloud properties simulated by the model are first evaluated using monthly mean observations of  
82 top-of-the-atmosphere fluxes, reflectance, cloud cover, and vertical structure (Section 3). A more advanced process-oriented  
83 evaluation is then conducted for tropical oceanic clouds based on the correlation between instantaneous cloud properties  
84 observed with the A-train. Illustrations of how this may help to improve model parameterizations are presented in Section 4.  
85 Conclusions are given in Section 5.

86

## 87 **2. Methodology**

### 88 2.1 The LMDZ5 climate model

89

90 LMDZ5 is the atmospheric component of the IPSL-CM5 climate model [Dufresne et al., 2013]. Two versions of this  
91 atmospheric model (LMDZ5A [Hourdin et al., 2013-a] and LMDZ5B [Hourdin et al., 2013-b]) are evaluated. Both model  
92 versions are described in cited papers and only key aspects are summarized here. LMDZ5A is similar to LMDZ4 [Hourdin

93 et al., 2006] used in the previous version of the IPSL model [Marti et al., 2010] but it has an increased vertical resolution  
94 (from 19 to 39 vertical levels), an improved representation of the stratosphere and a modified horizontal grid (1.895° in  
95 latitude x 3.75° in longitude). LMDZ5B is a new model version that includes, in addition to LMDZ5A, many new  
96 developments on the physical parameterizations such as (i) a new scheme of the boundary layer, which combines a model of  
97 turbulent diffusion and a 'mass flux' scheme in order to represent the coherent structures of the dry or cloudy convective  
98 boundary layer [Rio and Hourdin, 2008, Rio et al., 2010] and a new low-level cloud scheme [Jam et al., 2011], (ii) a  
99 parameterization of the cold pools created by re-evaporation of convective rainfall [Grandpeix and Lafore, 2010], and (iii) a  
100 modification of the triggering and the closure of the Emanuel (1991) convective scheme based on the Available Lifting  
101 Energy for the triggering and Available Lifting Power for the closure [Rio et al., 2013]. All model results have been  
102 obtained with multi-years simulations over the period 1979-2009 in which the sea surface temperature and the sea-ice cover  
103 are prescribed to values close to observations (AMIP experiments).

104

## 105 2.2. Observations

106

### 107 *Cloud cover and cloud vertical structure*

108

109 Thanks to its vertically resolved measurements, to its high sensitivity to optically thin atmospheric layers and to its high  
110 horizontal resolution, the CALIOP/CALIPSO lidar [Winker et al. 2007] is well suited to accurately identify clear sky areas,  
111 aerosol regions [Liu et al. 2008, Vuolo et al. 2009], fractionated cloud covers such as the trade winds cumulus [Konsta et al.,  
112 2012, Medeiros et al., 2010], optically thin clouds such as the sub-visible cirrus clouds [Sassen et al. 2008, Noel et al. 2010,  
113 Martins et al. 2011], polar stratospheric clouds [Noel et al. 2008, Pitts et al. 2007, Noel et al. 2010], and to document the  
114 cloud vertical distribution of the atmosphere.

115

116 In order to compare the GCM results with CALIOP observations, a dedicated product called CALIPSO-GOCCP has been  
117 developed to be fully consistent with the lidar simulator [Chepfer et al. 2010]. This product consists in applying Scattering  
118 Ratio (SR) thresholds values to the 532nm lidar SR signal to detect the presence of clouds. The cloud detection (0 or 1) is  
119 done at the original horizontal Level 1 CALIOP resolution (330m along track and 75m cross-track of the satellite orbit) but  
120 on a lower vertical resolution (40 equidistant vertical levels of 480 m height). The cloud fraction is then built on a 2°x2°  
121 latitude/longitude grid to provide information on cloud cover, on low- mid- and high-levels cloud covers, and on vertical  
122 cloud distributions.

123

124 *The monodirectional cloud reflectance: a surrogate for the cloud optical depth*  
125

126 The PARASOL instrument (POLDER-like, [Deschamps et al. 1994]) has a multi-viewing angle capability allowing for the  
127 estimation of the instantaneous monodirectional reflectance of clouds. The use of this level-1 product as a surrogate of the  
128 optical depth eliminates the need for many of the assumptions made during the retrieval process of the cloud optical  
129 thickness [Minnis et al., 1995]. The criteria used for the selection of the viewing angle are described below. Note that Cole  
130 et al. [2011] have computed and used CERES SW fluxes integrated over the diurnal cycle to perform a similar analysis but  
131 the PARASOL instantaneous monodirectional reflectance provides more precise information because it contains fewer  
132 assumptions than the CERES daily SW fluxes.

133

134 Above the ocean surface, the visible directional reflectance is defined as  $\rho(\theta_s, \theta_v, \phi_s, \phi_v) = \pi L(\theta_s, \theta_v, \phi_s, \phi_v) / E_s \mu_s$ , where  
135  $\theta_s, \theta_v, \phi_s, \phi_v$ , are respectively the solar zenith angle, the zenithal viewing angle, the solar and viewing azimuth angles,  $L$  is  
136 the measured radiance,  $\mu_s$  is the cosine of the solar zenith angle, and  $E_s$  the incident solar radiation. This directional  
137 reflectance is mostly sensitive to the solar zenith angle ( $\theta_s$ ), to the viewing direction ( $\theta_v, \phi_s - \phi_v$ ) and to the cloud optical  
138 depth. Some viewing directions are contaminated by the specular reflection of the solar light on the sea surface (i.e.  
139 sunglint), or are very dependent on cloud microphysical properties (e.g. particle shape through their optical properties). As  
140 the aim is to evaluate the optical depth, the reflectance observed in a single viewing direction that is mostly sensitive to the  
141 cloud optical depth and less to other parameters has been selected. The reflectance in a constant single direction has thus  
142 been selected all over the globe (Fig. A) in avoiding (i) directions with ( $90^\circ < \phi_s - \phi_v < 270^\circ$ ) since they are sensitive to the  
143 glitter reflection, (ii) the backscattering direction, which is highly sensitive to the cloud microphysical properties, and (iii)  
144 the nadir direction, which is less sensitive to the optical depth than any other direction. Among the others possible directions,  
145 the one at 865nm, which is the more frequently observed by PARASOL all over the globe ( $\theta_v = 27^\circ \pm 2.5^\circ, \phi_s - \phi_v = 320^\circ \pm 2.5^\circ$ )  
146 was selected. All the directional reflectance values of spatial resolution of  $6 \times 6 \text{ km}^2$  measured by PARASOL in this direction  
147 are then projected onto a  $2^\circ \times 2^\circ$  grid. The calibration of PARASOL is described by Fougnie et al. [2007]. The calibration  
148 accuracy is within 1.5% for the 865nm channel. The spatio-temporal sampling of PARASOL and CALIPSO observations is  
149 presented in Annex A.

150 Due to the difference of viewing angles and of pixel sizes between PARASOL and CALIPSO, cloudy and clear-sky  
151 properties cannot be separated at the pixel scale. The clear-sky and cloud properties are computed at the  $2^\circ \times 2^\circ$  scale  
152 following the methodology proposed by [Konsta et al., 2012]. The monodirectional reflectance  $R$  averaged over each grid

153 cell depends on the clear-sky reflectance (CSR), on the cloud cover (CC) and on the cloud reflectance (CR) in this grid cell  
154 according to the relation

$$155 \quad R = CC \times CR + (1-CC) \times CSR. \quad (2.1)$$

156 We assume that for each horizontal  $2^\circ \times 2^\circ$  grid cell, the fraction CC of the highest values of monodirectional reflectance  
157 observed at the pixel level correspond to cloudy conditions and the fraction (1-CC) of the lowest values correspond to clear-  
158 sky conditions. In practice, the cloud cover CC is first determined from CALIPSO observations daily and for each  $2^\circ \times 2^\circ$   
159 grid cell. Then, the cloudy monodirectional reflectance CR is computed as the grid cell average of the fraction CC of the  
160 highest values of monodirectional reflectance observed by PARASOL at the pixel level. The clear-sky monodirectional  
161 reflectance CSR is the grid cell average of the fraction (1-CC) of the lowest values. Note that the cloud reflectance used  
162 here is different from the total reflectance generally used and which contains the contribution of clear-sky surrounding  
163 clouds. Except stated otherwise, the results and figures based on CALIPSO and PARASOL observations are for the two-  
164 year period 2007-2008.

### 165 2.3. PARASOL and CALIPSO simulators

166  
167 By taking into account the effects of cloud overlap together with the specificities of the satellite, the model-to-satellite  
168 approach allows for a consistent comparison between the satellite observations described above (Section 2.2) and model  
169 outputs. The PARASOL and CALIPSO simulators have been designed for this purpose. The first step of the CALIPSO and  
170 PARASOL simulators consists in sub-gridding the model outputs (i.e. temperature, pressure, cloud cover, cloud condensate  
171 and effective radius of cloud droplets and ice crystals). The model vertical profiles are converted to an ensemble of subgrid-  
172 scale profiles by dividing each grid cell into a few tens of subcolumns generated randomly using the Subgrid Cloud Overlap  
173 Profile Sampler [Klein and Jakob 1999; Webb et al. 2001]. In each subcolumn, the cloud cover is assigned to be 0 or 1 at  
174 every model level with the constraint that the cloud condensate and cloud cover averaged over all subcolumns is consistent  
175 with the grid-averaged model diagnostics and the cloud overlap model assumption.

176  
177 The monodirectional reflectance, the total cloud cover and the vertical cloud distribution as it would be seen by PARASOL  
178 and CALIPSO respectively are then computed in each subcolumn (see Chepfer et al. 2008 for CALIPSO and Annex B for  
179 PARASOL) and averaged over each model grid cell. Due to the large and highly variable reflection of solar light on ground  
180 surfaces, the PARASOL simulator is not used above continents.

181 Above oceanic regions, the cloud monodirectional reflectance CR is computed for every grid cell at each time step, using  
182 the same definition as for the observations (Eq. 2.1) :

183 
$$CR = \frac{R - (1 - CC) \cdot CSR}{CC} \quad (2.2)$$

184 where the monodirectional reflectance R and the cloud cover CC have been previously computed by the simulator. The  
185 clear-sky reflectance has a fixed value in the simulator (CSR=0.03), which is consistent with the observations under clear-  
186 sky conditions [Konsta et al., 2012].

187 To simplify the post-processing of simulator outputs, the monodirectional reflectance is computed by the PARASOL  
188 simulator at every time step for a constant solar zenith angle corresponding to the A-train overpass at each latitude instead  
189 of the zenith angle corresponding to the local time in the GCM grid (Annex B). Sensitivity tests indicate that the cloud  
190 cover and reflectance computed by the PARASOL and CALIPSO simulator with the LMDZ model are almost insensitive to  
191 the frequency call of the simulator (every 1.5, 3, 6 hours), to the number of sub columns (if greater than 20 in each grid  
192 cell), and to the use of day or night time outputs (2% for the cloud cover and 2.5% for the reflectance; Figures not shown).  
193 In this study the simulator is called every 3 hours and 100 subcolumns are used.

194  
195 As the reflectance is not commonly used for cloud description, an approximate relationship between cloud reflectance and  
196 cloud optical thickness is given. The cloud reflectance (CR) can be converted in cloud optical thickness ( $C\tau$ ) using the  
197 coarse approximation of spherical particles when  $T > 0^\circ\text{C}$ , non-spherical particles when  $T < 0^\circ\text{C}$  and  $\theta_s = 30^\circ$  (see Annex B,  
198 Figure B.b). However, this cloud optical thickness should not be considered as the real cloud optical thickness but only as  
199 an approximation given for convenience. The rigorous comparison between models and observations should be made using  
200 the monodirectional reflectance. The same assumption to convert PARASOL cloud reflectances into cloud optical  
201 thicknesses are made for both observed and simulated data in order to make sure that this conversion does not introduce an  
202 artifact when comparing models and observations.

203 PARASOL and CALIPSO simulators are included in COSP (CFMIP Observational Simulator Package) [Bodas-Salcedo et  
204 al. 2011], which also includes other simulators such as the ISCCP [Klein and Jakob 1999; Webb et al. 2001] and the  
205 CloudSat [Haynes et al. 2007] simulators. The COSP simulator is available to the community via the Cloud Feedback  
206 Model Intercomparison Project (CFMIP) web page ([cfmip.net](http://cfmip.net)) and the monthly and instantaneous datasets used here,,  
207 which are consistent with the COSP outputs, are available via the “CFMIP Observations for Model evaluation” website  
208 ([climserv.ipsl.polytechnique.fr/cfmip-obs.html](http://climserv.ipsl.polytechnique.fr/cfmip-obs.html)).

209

### 210 3. Assessment of cloud properties using monthly mean statistics

211

212 The basic properties of clouds simulated by climate models are usually evaluated by comparing monthly mean values of the  
213 observed TOA fluxes, cloud cover, cloud optical depth and cloud top height (ie. Zhang et al. 2005, Klein et al. 2013). In this  
214 section, this approach based on monthly mean statistics is followed to evaluate the two versions of the LMDZ climate  
215 model.

#### 216 **a) Cloud geographical distribution**

217 An aim of the improvements in the LMDZ5B model compared to LMDZ5A was to improve the cloud cover [Hourdin et al.,  
218 2013-b] and this has been achieved in many regions. The cloud cover (CC) simulated by LMDZ5B is in better agreement  
219 with observations than the CC simulated by LMDZ5A over the North Pacific and the North Atlantic, over the warm pool  
220 (where there are high convective clouds), along the East coast of the oceans and over the trade wind regions (where cumulus  
221 clouds dominate) but the CC values are still too low (Annex C). When considering the zonal mean values, LMDZ5B still  
222 underestimates the cloud cover in the tropics even though the bias is reduced by a factor of two compared to LMDZ5A.

223 High-level clouds feature a better vertical distribution in LMDZ5B than in LMDZ5A with a lower cloud cover but this CC  
224 is still too high (Annex C). LMDZ5B is able to simulate mid-level clouds even though they are still too few. Low-level  
225 clouds are also better simulated in LMDZ5B with a larger cloud cover but the low-level clouds are too low and they are too  
226 concentrated in one single layer. At middle and high latitudes, LMDZ5B simulates relatively well the large vertical extent of  
227 the frontal clouds associated with storms. The cloud fraction is improved in LMDZ5B compared to LMDZ5A but the cloud  
228 reflectance is not. Cloud reflectance and therefore cloud optical thickness are strongly overestimated by both model versions  
229 almost everywhere and in particular over the subtropical oceans and in mid and high latitudes (Annex C).

#### 230 **b) Tropical oceanic clouds in dynamical regimes**

231  
232 Based on their geographical distribution the cloud properties discussed in the previous sections can be summarized in the  
233 tropics using dynamical regimes [Bony et al., 2004]. Figure 1 shows the monthly mean cloud cover (Fig. 1a), cloud  
234 reflectance (Fig. 1b) and SW albedo (Fig. 1c) as a function of the monthly mean vertical velocity at 500hPa ( $\omega_{500}$ ), as well  
235 as the PDF of  $\omega_{500}$  (Fig. 1d) over the tropical ocean. In the convective regions ( $\omega_{500} < 0$ ), the cloud cover simulated by  
236 LMDZ5B is closer to observations than the cloud cover simulated by LMDZ5A whereas in subsidence regions where  
237  $\omega_{500} > 20$  hPa/day, the cloud cover is underestimated in both model versions (Fig. 1a). The cloud reflectance is strongly  
238 overestimated in both model versions, this overestimation being smaller in convective regions where  $\omega_{500} < -40$  hPa/day  
239 (Fig. 1b). Despite these large discrepancies, both model versions simulate reasonably well the SW albedo in subsidence

240 regions ( $\omega_{500} > 0$ , Fig. 1c), which dominates in the Tropics (65% of the surface of the entire tropical belt). Even though both  
241 model versions reproduce well the mean value and the overall geographical pattern of the albedo (Figures not shown), they  
242 do not succeed in simulating properly the cloud cover and the cloud reflectance.

### 243 **c) Correlation between cloud top pressure and cloud optical thickness over the tropical ocean**

244

245 The joint histograms of cloud top pressure (CTP) and cloud optical thickness ( $C\tau$ ) obtained with ISCCP data [Rossow and  
246 Schiffer, 1991] have been widely used for atmospheric studies [e.g. Jakob and Tselioudis 2003, Rossow et al. 2005] and for  
247 model evaluation [e.g. Webb et al, 2001, Williams and Tselioudis, 2007, Klein et al., 2013]. They are computed using two  
248 methods. In the first method, the ISCCP-D2 data and ISCCP simulator outputs are directly used (Fig. 2d-f). In the second  
249 method, the CALIPSO and PARASOL data and simulator outputs are used and CTP is defined as the pressure of the highest  
250 level where the instantaneous CALIPSO-GOCCP cloud cover in each  $2^\circ \times 2^\circ$  grid cell is greater than 0.1 (Fig. 2a-c).  
251 Sensitivity tests show that results are not very sensitive to the value of this threshold when it varies from 0.1 to 0.3. The  
252 cloud optical thickness  $C\tau$  is computed from the cloud reflectance. The 2D histogram features these instantaneous CTP and  
253  $C\tau$  data for each grid cell and averaged over time.

254

255 The histogram based on ISCCP data (Fig. 2d) is very different from the one based on CALIPSO-PARASOL data (Fig. 2a).  
256 The 2D histogram over the tropical ocean obtained with the observed CALIPSO-GOCCP and PARASOL data (Fig. 2a)  
257 features two distinct populations, the first one in the high troposphere and the second one in the low troposphere. The  
258 histogram based on ISCCP data features a single cluster in the middle of the troposphere. This difference is a direct  
259 consequence of the much-improved measurement of cloud height by active sensors (CALIPSO) compared to passive ones  
260 (ISCCP), as already shown by Chepfer et al. [2008]. A more advanced comparison between ISCCP and merged CloudSat  
261 and CALIPSO histograms is described in Mace and Wrenn [2013].

262

263 Similar features are also visible in the model results where two populations of low and high clouds are featured when using  
264 the CALIPSO and PARASOL simulators (Fig. 2.b-c) and one single cluster of high clouds is featured when using the ISCCP  
265 simulator (Fig. 2.e-f). The main biases of the models (e.g. too many high clouds, too few low clouds, too high cloud optical  
266 thickness) also appear when using ISCCP observed and simulated data. However low clouds can be evaluated using  
267 CALIPSO but they do not occur when the ISCCP simulator is applied. Similarly, the optically thin clouds can be evaluated  
268 using CALIPSO but they are not detected in ISCCP observations nor simulated by the ISCCP simulator.

269 **4. An advanced “process oriented” evaluation of tropical clouds description taking full advantage of the A-train**  
270 **capability**

271

272 4.1 The added value of evaluating the model using instantaneous cloud properties

273 For climate change and climate variability studies, it is important to characterize and assess how cloud properties vary as a  
274 function of atmospheric variables describing the clouds environment. For example in climate feedbacks studies, changes  $\Delta E$   
275 of the cloud environment variables are assumed to depend on the change  $\Delta T$  of the surface temperature (e.g. Colman and  
276 McAvaney, 1997, Soden and Held, 2006, Bony et al., 2006) and cloud properties are therefore assumed to vary as a function  
277 of the surface temperature. Within this framework, various studies (e.g. Bony et al., 2004, Webb et al., 2006) have analyzed  
278 how the cloud radiative effects vary in response to a change of the surface temperature at inter-annual time scales or under  
279 climate change situations. This approach has been successful to improve our understanding of cloud feedbacks but the  
280 temporal scale used in those studies (in general monthly mean variables) does not allow for the understanding of the direct  
281 relationship between these results and the model parameterizations. Indeed, cloud properties vary instantaneously in  
282 parameterizations (or with small time constants) when variables describing the environment (e.g. atmospheric stability,  
283 humidity) vary. These dependencies between cloud and environment characteristics are highly non-linear so that the  
284 relationship between these instantaneous variables may be very different from the relationship between their monthly or  
285 seasonal mean values. The A-Train offers new possibilities to analyze the correlation between instantaneous cloud cover and  
286 cloud reflectance in more detail.

287

288 Assuming for simplicity reasons that the clear-sky reflectance over ocean is negligible, the variation  $\Delta R$  of the reflectance  $R$   
289 (eq. 2.1.) depends on how the cloud cover ( $CC$ ) and the cloud reflectance ( $CR$ ) vary:

290 
$$\Delta R \approx CR.\Delta CC + CC.\Delta CR.$$

291 The variation  $\Delta R$  will be very different if the variations  $\Delta CC$  and  $\Delta CR$  have the same or the opposite sign. The  $CC$  and the  
292  $CR$  variables estimated at the same time and location, as well as their joint variations are analyzed with a focus on the case  
293 where they vary in the same or opposite way. An evaluation of how cloud properties vary with the environment is more  
294 constraining for the models than an evaluation of the mean state and this may be one way to increase the confidence in  
295 model results.

296

297 The relationship between cloud cover and optical thickness over the tropical oceans is shown in Figure 3. In observations,  
298 this relationship has been shown to be significantly different when using monthly or instantaneous values [Konsta et al.,  
299 2012]. When using monthly mean data (Fig. 3, lower line), the observations show an almost linear relationship between the

300 two variables: as the cloud cover increases, the cloud optical depth increases too (Fig. 3-d). The two versions of the model  
301 show very different behaviors from what is observed: the cloud optical depth remains almost constant when the cloud cover  
302 varies. LMDZ5A does not simulate the highest values of cloud cover and the simulated cloud reflectance is too high on  
303 average (Fig. 3-e). LMDZ5B simulates clouds that have a large cover and a reflectance consistent with observations, but  
304 clouds with a small cover have a too large reflectance (Fig. 3-f).

305

306 The use of instantaneous data gives a more accurate picture of the relationship between cloud cover and cloud optical depth  
307 and, for the models, a very different picture from what is observed (Fig. 3, upper line). For the observations, there is a  
308 tendency of increasing cloud reflectance with increasing cloud cover as it is the case for monthly mean values. But the  
309 instantaneous data reveal two separate cloud populations: one with a low cloud cover ( $CC < 60\%$ ) and a low reflectance  
310 ( $CR < 0.2$ ) and another one with a cloud cover close to 1 and a cloud reflectance value ranging from 0.1 up to 0.9 (Fig. 3-a).  
311 Intermediate cloud reflectance (0.2-0.4) and cloud cover (0.5-0.8) values occur when using monthly mean values but are  
312 much less frequent when using instantaneous values. These intermediate values therefore do not correspond to actual  
313 clouds. Both model versions simulate clouds with a low cover but their reflectances are much too high (Fig. 3-b,c).  
314 LMDZ5A simulates few clouds with a cover close to one whereas LMDZ5B simulates many clouds with a cover close to  
315 one, as observed. However, the cloud reflectance-cloud cover relationship for both model versions does not show an  
316 increase of the cloud reflectance with cloud cover, as this is the case in the observations. The LMDZ5B model even shows  
317 an opposite relationship.

318

319 The instantaneous correlation between cloud variables constitutes a key test to improve the confidence in how cloud  
320 properties simulated by climate models vary in changing situations. Fig. 3 clearly shows that this test is highly challenging.  
321 Instantaneous cloud properties are analyzed below.

322 4.2. Evaluation of tropical clouds using instantaneous clouds properties

#### 323 4.2.a Optical thickness of clouds and their vertical distribution

324 The PDF of the cloud reflectance (CR) observed by PARASOL, and simulated by the model and by the PARASOL  
325 simulator (Figure 4a), confirms that both model versions strongly overestimate the cloud reflectance. The cloud population  
326 is divided into three different classes according to their optical thickness: (i) the optically thin and intermediate clouds  
327 ( $CR < 0.2$ , i.e.  $C\tau < 3.41$ ) corresponding to 55%, 29% and 25% of the clouds for the observations, the LMDZ5A and the  
328 LMDZ5B model respectively, (ii) optically thick clouds ( $0.2 < CR < 0.5$ , i.e.  $3.41 < C\tau < 11.42$ ) corresponding to 34%, 50% and  
329 53% of the clouds for the observations, LMDZ5A and LMDZ5B respectively, and (iii) very thick clouds ( $CR > 0.5$ , i.e.

330  $C\tau > 11.42$ ) corresponding to the less populated class: 11%, 21% and 22% for the observations, LMDZ5A and LMDZ5B  
331 respectively. The mean vertical profile of the cloud fraction observed from CALIPSO-GOCCP and simulated by the model  
332 and by the simulator is shown on Fig.4b-d for the three cloud classes. Note that the cloud reflectance is a vertically  
333 integrated value and characterizes the whole atmospheric column, while the cloud fraction is a local value at each vertical  
334 level. For optically thin and intermediate clouds (i.e. when  $C\tau < 3$  or  $CR < 0.2$ ) the lidar traverses clouds and provides  
335 information for the whole atmosphere whereas for thicker clouds ( $CR > 0.2$ ) the lidar signal is attenuated and does not  
336 provide information below the higher thick clouds.

337  
338 Observations show that optically thin and intermediate clouds ( $CR < 0.2$ , i.e.  $C\tau < 3.4$ , Fig.4b) are mainly low-level clouds  
339 with low values of cloud fraction ( $CF \approx 0.15$ ). For the same range of optical thickness, both versions of the model simulate  
340 high-level clouds with intermediate values of the cloud fraction ( $CF \approx 0.27$ ). LMDZ5A does not simulate any low-level  
341 clouds while LMDZ5B simulates some but too few of them ( $CF < 0.05$ ). For optically thick clouds ( $0.2 < CR < 0.5$ , Fig.4c),  
342 both model versions correctly simulate high-level clouds with a mean cloud fraction ( $CF \approx 0.17$ ) and altitude close to the  
343 observations. Both model versions simulate low clouds with a correct fraction but a too low altitude, and they fail to  
344 simulate mid-level clouds. Lastly, optically very thick clouds ( $CR > 0.5$ , Fig.4d) are mainly high-level clouds with a large  
345 cloud fraction ( $CF \approx 0.37$ ) with some mid-level clouds ( $CF \approx 0.2$ ) and only a few low-level clouds. The two model versions  
346 simulate optically very thick clouds with a very different cloud vertical structure, with much less high-level clouds  
347 ( $CF \approx 0.15$  for LMDZ5A and 0.06 for LMDZ5B), almost no mid-level clouds and a fraction of low-level clouds ( $CF \approx 0.1$ )  
348 close to observations, also smaller.

349  
350 In summary, the fraction of mid- and high-levels clouds increases with the cloud reflectance in the observations but  
351 decreases in the models. The fraction of low-level clouds in the observation and in the models does not show a tendency of  
352 change with cloud reflectance, and the altitude of the simulated clouds is generally too low.

#### 353 **4.2.b. Focus on high-level clouds**

354 In ascent regions,  $2^\circ \times 2^\circ$  grid cells with no high-level clouds ( $P < 440$  hPa) are rarely observed (15% of the time, Fig. 5-a) and  
355 rarely simulated by both models (10 to 20% of the time). The cumulative distribution function (CDF) of high-level cloud  
356 cover regularly increases (their frequency of occurrence is almost constant) until it becomes close to one. For these very  
357 cloudy conditions, there is a rapid increase in the CDF. The frequency of occurrence is much larger (typically 5 to 10 times)  
358 when the cloud cover is close to 1 than when it is smaller. The cloud cover of high-level clouds is larger than 95% in more  
359 than 25% of the situations. LMDZ5A simulates too few of these high-level clouds with a large cover but simulates too many

360 high-level clouds with a too low cover compared to observations. On the contrary, LMDZ5B simulates too many high  
361 clouds with a large cover and the high-cloud cover is larger than 95% in 40% of the situations. Situations with almost no  
362 high-level clouds are much more frequent in subsidence regions ( $\approx 40\%$  of the cases, Fig. 5-b) than in ascent regions and  
363 situations with a large cover of high-level clouds are rare. Both model versions simulate the observed general behaviors of  
364 clouds although LMDZ5B is closer to observations. The normalized cloud cover of high-level cloud is now used to show  
365 how the different height categories (here, high clouds) are divided among all observed clouds [Stubenrauch et al., 2012].  
366 The normalized cloud cover of high-level cloud is defined as  $NCC\_high = CC\_high/CC$ , where  $CC\_high$  is the cloud cover  
367 of high-level clouds and  $CC$  is the total cloud cover [Konsta et al., 2012]. In ascent regions, the observed normalized high-  
368 cloud cover regularly increases with the total cloud cover (except for very small cloud cover) and reaches values close to  
369 one in fully overcast situations (Fig. 5-c). When the total cloud cover is small the high-level clouds have a small  
370 contribution to the total cloud cover, which means that mid- and low-level clouds dominate. On the contrary, high-level clouds  
371 dominate when the cloud cover is close to one. In LMDZ5A, high-level clouds always dominate even when the total cloud  
372 cover is small. This model fails to simulate enough mid- and low-level clouds in ascent regions. This bias is also in  
373 LMDZ5B but to a much lesser extent. In subsidence regions, the observed normalized high cloud cover is small and  
374 increases with the cloud cover (Fig. 5-d). Low-level clouds dominate, as expected. Both model versions simulate a too large  
375 normalized cover of high clouds, which is consistent with a too small value of the low-level cloud cover in these regions.

#### 376 **4.2.c. Focus on boundary layer clouds**

377 Low-level clouds over the tropical oceans are now examined. To do so, only the atmospheric columns where low-level  
378 clouds are dominant are considered. These columns are defined as the  $2^\circ \times 2^\circ$  grid cells where the normalized cover of low-  
379 level clouds ( $P > 680$  hPa) is greater than 90% ( $CC\_low/CC > 90\%$ ). Figure 6 presents the relationship between the cloud  
380 cover and the cloud reflectance in these situations. The observed clouds may be organized in two groups (Fig. 6-a). In the  
381 first group, clouds have a small cover and a small reflectance. Further analysis shows that these clouds are present all over  
382 the tropics, with the most dominant population confined in the trade cumulus regions. Their properties are consistent with  
383 those of small cumulus clouds. The second group is composed of clouds with cover close to one and with a large reflectance  
384 ( $0.3 < CR < 0.6$ ), i.e. a large optical thickness ( $5.5 < C\tau < 17$ ). They are mainly located on the east coast of the tropical oceans  
385 and their properties are consistent with those of stratocumulus clouds. The results shown in Fig 6-a are broadly consistent  
386 with those obtained by Cole et al. [2011] using CERES and MODIS observations (their Fig. 7). The LMDZ5A model results  
387 show very different characteristics (Fig. 6-b) with most of the low-level clouds having a too large cloud cover and a too  
388 large reflectance, i.e. a too large optical thickness. The LMDZ5B model simulates two clusters of low-level clouds, one with  
389 small cloud cover values and another one with a cloud cover close to one, which is more consistent with observations.

390 However, when the cloud cover is small, the reflectance is much too large and increases when the cloud cover decreases,  
391 unlike in the observations.

392

393 This relationship is further examined by focusing on specific cloud regimes, following the methodology proposed by  
394 Medeiros and Stevens [2011] that allows for a separation in stratocumulus and shallow cumulus regimes. The stratocumulus  
395 regime corresponds to a regime where clouds have the largest values of cloud cover and cloud reflectance both in the  
396 observations and in the model. The shallow cumulus regime corresponds to clouds with smallest values of cloud cover and  
397 cloud reflectance (Figures not shown). For the stratocumulus regime, the observed relationship between cloud cover and  
398 cloud reflectance is quasi linear. The same relationship is also examined using the ISCCP 3hourly observations on the  $2^\circ \times 2^\circ$   
399 grid and the ISCCP simulator (Fig. 6d,e,f). The ISCCP cloud optical thickness is converted into cloud reflectance by  
400 assuming a fixed solar zenith angle  $\theta_s = 30^\circ$  and spherical particles. The results from ISCCP are consistent with those  
401 obtained with CALIPSO-PARASOL, both for the observations and the models. However, the confidence in CALIPSO-  
402 PARASOL data is higher because the detection of low-level clouds is much better compared to ISCCP, as noted above. In  
403 CALIPSO-PARASOL data, cumulus clouds are found to have larger values of cloud cover compared to ISCCP  
404 observations. The decrease of cloud reflectance with cloud cover observed with CALIPSO-PARASOL is not evident with  
405 ISCCP.

406

407 According to theory and observation, the cloud optical thickness increases with the cloud top height for low-level clouds of  
408 same base height: as the cloud grows vertically, there is more water to condensate and the cloud optical depth increases.  
409 This relationship is a function of many phenomena (e.g. turbulent mixing, precipitation efficiency) that are not accurately  
410 known. This motivated many field campaigns [e.g. Coakley et al., 2005, Siebesma et al., 2003]. The analysis of this  
411 relationship on the global scale is performed using the CALIPSO-PARASOL observations. Figure 7 shows the mean cloud  
412 reflectance as a function of the cloud top pressure when low-level clouds are dominant. The cloud top pressure is defined as  
413 the first layer going downward from the 680hPa where the cloud cover is greater than 0.1. Both model and observations  
414 show that the cloud optical depth increases with cloud top altitude, as expected. However, the cloud optical thickness  
415 simulated by the models is two to three times larger than the observed one.

416

417 The poor representation of the low-cloud properties by the models may have important consequences for climate change  
418 studies. Indeed, low-level clouds cover most of the tropical ocean and are the main source of spread in climate sensitivity  
419 estimates [Bony and Dufresne, 2005; Vial et al., 2013]. In addition, the amplitude of the low-level cloud feedback depends

420 on the cloud radiative effect [Brient and Bony, 2012] and an error in the later may impact the value of the former.

421

### 422 **4.3. From model evaluation to model improvement**

423

424 The analysis of monthly mean values confirm that the LMDZ5 model, as many other models, simulate low-level clouds  
425 with a too low cloud cover and a too high optical thickness (Nam et al. 2012, Klein et al. 2013). The use of instantaneous  
426 values further highlights the fact that the mean values as well as the variation of the cloud optical thickness with the cloud  
427 cover in the LMDZ model were biased. Key deficiencies in the model parameterizations can be identified and improved  
428 using the diagnostics presented above. Presenting new parameterizations for low-level clouds is far beyond the scope of this  
429 paper but the proposed diagnostics are very relevant for future model developments. The major discrepancy in models  
430 compared to observations identified above with increasing optical thickness as the cloud cover decreases, (Fig. 6) is further  
431 analyzed in the LMDZ5A model.

432

433 Many factors affect both the cloud cover and the cloud reflectance but a sensitivity analysis shows that the main driver of  
434 the erroneous relationship between these two variables in the LMDZ5A model is the liquid water content and not the micro-  
435 physic properties of clouds such as the cloud droplet size. The vertical integrated cloud water amount (or liquid water path)  
436 for low-level clouds increases as the cloud cover increases, like the cloud reflectance increases as the cloud cover increases,  
437 and the liquid water path is strongly correlated with the cloud reflectance (Figure 8-a).

438

439 The cloud fraction and liquid water content in the LMDZ5A model are diagnosed from the large-scale value of the total  
440 (vapor + condensed) water  $Q_t$ , the moisture at saturation  $Q_s$ , and the subgrid scale variability of the total water using a  
441 generalized log-normal Probability Distribution Function (PDF) defined by three statistical moments (mean, variance,  
442 skewness) (Bony and Emanuel, 2001 ; Hourdin et al., 2006). This parameterization was originally developed for convective  
443 clouds and then applied for all cloud types. Off-line calculations show that the increase of cloud reflectance when  
444 decreasing cloud cover (Fig. 6-b) cannot be explained under the conditions that generally exist when low-level clouds are  
445 present. This increase of cloud reflectance when the cloud fraction decreases is due to the deep convection scheme, which  
446 was activated quite frequently, without producing any deep convective clouds but affecting the PDF of the total water  
447 content at low level and therefore the cloud properties there. Sensitivity simulations confirm this hypothesis and show that  
448 the cluster of points in the upper left part of Fig. 6-b with high cloud reflectance and low cloud cover no longer exists when  
449 the deep convection scheme is switched off. However, the observed increase of reflectance with cloud cover is not

450 reproduced by the model.

451

452 An implicit assumption of most (if not all) PDF parameterization approaches is that the sub-grid cloud cover is  
453 homogeneous (i.e. is either 0 or 1) in the vertical in each atmospheric layer. This assumption may be relevant when the sub-  
454 grid total water content is far above or far below the moisture at saturation but it may be questionable when the two values  
455 are similar. A very simple test is therefore performed to check the sensitivity of the cloud characteristics to this assumption.  
456 The equation for the liquid water content is assumed to be unchanged and clouds are assumed to only cover a vertical  
457 fraction of the atmospheric layer when the sub-grid humidity is close to the saturation and that this vertical fraction varies  
458 linearly from 0 when  $Q_t = Q_s - \Delta Q$  to 1 when  $Q_t = Q_s + \Delta Q$ . In practical terms, the only change is to use  $Q_s - \Delta Q$  instead of  $Q_s$   
459 in the cloud cover formula. For the vertical spread of the humidity  $\Delta Q$ , the same value as the one used to characterize the  
460 horizontal spread of humidity (Hourdin et al., 2006) is used. The typical values of  $\Delta Q/Q_t$  are about a few percent and are  
461 comparable with the change of  $Q_s$  due to the vertical gradient of temperature within an atmospheric layer. These values of  
462 the vertical spread of humidity are assumed to be realistic even though this choice is arbitrary and only relevant for a  
463 sensitivity test. The impact of this change on the cloud cover and on the relationship between cloud cover and cloud  
464 reflectance is very large for all clouds (Fig. 8-b to compare with Fig. 3 -b) and for conditions where low-level clouds are  
465 dominant (Fig. 8-c to compare with Fig. 6-b). Above all, the cloud reflectance increases with the cloud cover, which is  
466 consistent with observations and opposite to the results obtained with the original parameterization. A direct consequence is  
467 a modification of the SW flux at the TOA of about  $10 \text{ W/m}^{-2}$ . The geographical distribution of the simulated cloud  
468 reflectance is much closer to the observed values and the cloud cover is more realistic with more mid- and low-level clouds  
469 simulated, which is closer to the observed vertical structure of clouds. Although much more work is required to develop a  
470 new parameterization, the sensitivity test presented here illustrates the fact that the diagnostic is accurate enough to help  
471 identifying the origins of a major problem in the simulated low-level cloud properties and to show the direct effect of a  
472 specific modification of the model parameterizations.

473

474 Various studies have already analyzed how the effect of sub-grid heterogeneity of cloud properties may affect the  
475 parameterization of cloud radiative properties [e.g. Barker and Wielicki, 1997; Li et al. 2005] or autoconversion rate [e.g.  
476 Kawai and Texeira, 2012; Boutle et al., 2014], but very few have analyzed the effect of sub-grid heterogeneity of cloud  
477 properties on the parameterization of cloud cover even though this possibly large effect has been recognized [Pincus and  
478 Klein, 2000]. Based on results obtained with large eddy simulation (LES) models, Neggers et al. [2011] found that this  
479 effect is large for cumulus cloud type, which is consistent with the present hypothesis. To our knowledge few (if any)

480 atmospheric models consider this phenomena in their parameterization. The possible role of this simplification on the  
481 tendency of models to simulate too few and too bright clouds deserve further investigation and is beyond the scope of this  
482 study.

## 483 **5. Summary and conclusion**

484

485 An evaluation of cloud characteristics (e.g. cloud cover, cloud vertical distribution and cloud optical depth) simulated by  
486 two versions of the LMDZ5 GCM using observations from PARASOL and CALIPSO has been presented. Model and  
487 observations have been compared using “observations simulators”, which allow direct comparisons between modeled and  
488 level 1 observed data by taking into account the spatial scale differences between model and observations and by avoiding  
489 most of the *a priori* hypothesis usually made in retrieval algorithms. This evaluation was performed using both monthly  
490 mean and instantaneous values and it has been shown how the latter allows for further analysis and may be used to help  
491 improve cloud parameterizations.

492

493 The comparison between the two versions of the LMDZ5 model and PARASOL/CALIPSO observations using the monthly  
494 mean climatologies clearly shows an improvement in the representation of cloud cover and cloud vertical distribution of  
495 LMDZ5B compared to LMDZ5A. This improvement consists of an increase of the cover of the boundary layer clouds  
496 especially in the trade wind regions, an improvement of the altitude and, to a less extent, of the fraction of the high-level  
497 clouds and the simulation of the large vertical extent of the frontal clouds associated with storms in the middle and high  
498 latitudes. Although reduced, some model biases in LMDZ5A are still present in LMDZ5B and are generally shared with  
499 many climate models, such as the lack of mid-level clouds in the mid latitudes [Chepfer et al., 2008, Zhang et al., 2005], the  
500 presence of optically too thick high-level clouds all around the globe [Zhang et al., 2005], and the lack of boundary layer  
501 clouds all around the tropical belt (in particular in the trade wind regions). Both versions of LMDZ5 model simulate the SW  
502 albedo well although they strongly overestimate the cloud optical depth. This suggests some compensating error between  
503 the cloud cover and the cloud optical depth and this compensation is different for the two model versions.

504

505 When using the instantaneous relationship between the cloud properties, new features appear and more precise conclusions  
506 may be drawn. Over the tropical oceanic regions, the following results are obtained:

507 1. Observed clouds are grouped in two clusters, one where clouds have a low to mid cover ( $CC < 60\%$ ) and a low reflectance  
508 ( $CR < 0.2$ ) and another one with a cover close to 1 and a reflectance that ranges from 0.1 to 0.9. The two model versions  
509 reproduce these two clusters but with a lack of fully overcast situations ( $CC = 1$ ) in LMDZ5A. In both model versions, there

510 are too few clouds with a small cover and their reflectance is strongly overestimated. There is a general tendency of  
511 increasing cloud reflectance with increasing cloud cover in observations and the models do not reproduce this tendency.  
512 Note that the relation between cloud fraction and cloud optical thickness are very different when using monthly mean or  
513 instantaneous values both in observations and in the models.

514 2. The CALIPSO-GOCCP data allow for a detailed description of the vertical distribution of clouds. In the observations, the  
515 fraction of mid- and high-levels clouds increases with the all clouds reflectance, whereas it decreases in the models. In  
516 ascent regions, there are frequent situations where grid cells are fully overcast with high-level clouds ( $CC_{high} > 95\%$ ): 25%  
517 in observations, 10% and 40% in LMDZ5A and LMDZ5B respectively. In observations high-level clouds co-exist with low-  
518 and mid-level clouds whereas the multi-layer clouds are much less frequent in models.

519 3. The tropical low-level cloud properties can be grouped in two clusters. The first one corresponds to cumulus-type clouds  
520 and the second one corresponds to stratocumulus-type clouds. Observations show that the cloud optical depth increases with  
521 cloud cover and none of the model versions reproduce this general trend; they may even feature an opposite trend. Both  
522 models underestimate the low-level cloud cover but overestimate their reflectance. They do not produce enough low-level  
523 clouds and the low-level clouds they produce are too thick. These two biases partly compensate each other when  
524 considering the SW albedo. On average, the altitude of the low-level clouds simulated by the models is too low.

525 4. The relationship between instantaneous cloud cover and cloud reflectance for low-level clouds may be directly compared  
526 to what is expected from the parameterizations in these conditions. This diagnostic allows for the identification of key  
527 deficiencies in the parameterization and their origin as well as for possible improvements. More precisely, part of the  
528 problem is due to intermittent triggering of the convection and another part of the problem is due to a too large in-cloud  
529 liquid water amount. For the latter, the origin of the problem is believed to be the assumption of current parameterization  
530 that the cloud covers is homogeneous all along the vertical in each atmospheric layer. Sensitivity tests were performed and  
531 have shown that suppressing this assumption may have a large impact, leading to potential improvements in the cloud  
532 characteristics. More work is required to go from these sensitivity experiments to establishing useful new parameterizations.

533

534 Multi-instrument missions like the A-train offer the possibility to observe many properties of the clouds and their  
535 environment, which allows for a better evaluation of the climate simulated by atmospheric models. Beyond the separate  
536 analysis of each variable, the analysis of their joint variations allows for a deeper analysis and a better understanding of the  
537 dominant physical processes driving cloud properties. This is the case when using monthly mean values and using  
538 instantaneous data is even more powerful. Even if the instantaneous observations are less precise than averaged values and  
539 even if the collocation procedure may lead to the rejection of many observations, the analysis of their joint variations allows

540 for a more precise evaluation of cloud properties, it may highlight new features or problems, it may facilitate the link  
541 between observations and parameterizations. It may also help to bridge the gap between model evaluation and model  
542 development.

543

#### 544 *Acknowledgments*

545 The authors would like to thank CNES and NASA for the PARASOL and CALIPSO data, CGTD/ICARE for the collocation  
546 of the CALIOP L1 and PARASOL L1 datasets, Climserv/ICARE for the data access and for the computing resources. This  
547 research was partly supported by the FP7 European projects EUCLIPSE (# 244067) and IS-ENES2 (#312979). We also  
548 thank D. Tanré and F. Ducos for providing PARASOL monodirectional reflectance observations, Michel Viollier for fruitful  
549 discussions on CERES and PARASOL data, Michel Capderou for his useful comment on the A-train orbit, J. Riedi for its  
550 help to built Fig. 1A, and S. Bony for useful discussions. We strongly acknowledge the editor and the reviewers for their  
551 numerous suggestions that have helped us to improve the manuscript.

552

## 553 **References**

554

- 555 Barker HW, Wielicki BA., 1997. Parameterizing grid-averaged longwave fluxes for inhomogeneous marine boundary layer  
556 clouds. *J. Atm. Sci.* 54(24): 2785-2798.
- 557 Bodas-Salcedo A, M. J. Webb, S. Bony, H. Chepfer, J.-L. Dufresne, S. A. Klein, Y. Zhang, R. Marchand, J. M. Haynes, R.  
558 Pincus, V. O. John, 2011: COSP: satellite simulation software for model assessment. *Bull. Amer. Met. Soc.*, 92(8),  
559 doi:10.1175/2011BAMS2856.1
- 560 Bony S., J.-L. Dufresne, H. Le Treut, J.-J. Morcrette and C. Senior, 2004 : On dynamic and thermodynamic components of  
561 cloud changes. *Clim. Dyn.*, 22, 71-86.
- 562 Bony S. and J.-L. Dufresne, 2005: Marine boundary layer clouds at the heart of tropical cloud feedback uncertainties in  
563 climate models, *Geophys. Res. Lett.*, 32, No. 20, L20806, doi:10.1029/2005GL023851.
- 564 Bony S., R. Colman, V. M. Kattsov, R. P. Allan, C. S. Bretherton, J.-L. Dufresne, A. Hall, S. Hallegatte, M.M. Holland, W.  
565 Ingram, D. A. Randall, B.J. Soden, G. Tselioudis and M. J. Webb, 2006: How well do we understand and evaluate  
566 climate change feedback processes? *J. Climate*, 19, 3445-3482.
- 567 Boutle IA, Abel SJ, Hill PG, Morcrette CJ., 2014. Spatial variability of liquid cloud and rain: observations and  
568 microphysical effects. *Q. J. R. Meteorol. Soc.* 140: 583-594. DOI:10.1002/qj.2140
- 569 Brient F. and S. Bony, 2012: How may the low-cloud radiative properties simulated in the current climate influence the low-  
570 cloud feedbacks under global warming? *Geophys. Res. Lett.*, 39, L20807, doi:10.1029/2012GL053265.
- 571 Cesana G. and H. Chepfer, 2013: Evaluation of the cloud thermodynamic phase in a climate model using CALIPSO-  
572 GOCCP. *Geophys. Res. Lett.*, 118,7922-7937, doi:10.1002/jgrd.50376.
- 573 Coakley J.A., M.A. Friedman and W.R. Tahnk, 2005: Retrievals of cloud properties for partly cloudy imager pixels. *J.*  
574 *Atmos. Ocean. Tech.* 22, 3-17.
- 575 Cole J., H. W. Barker, N. G. Loeb, K. von Salzen, 2011: Assessing Simulated Clouds and Radiative Fluxes Using Properties  
576 of Clouds Whose Tops are Exposed to Space. *J. Climate*, 24, 2715-2727, doi: 10.1175/2011JCLI3652.1
- 577 Colman R. and B. J. McAvaney, 1997: A study of general circulation model climate feedbacks determined from perturbed  
578 SST experiments. *J. Geophys. Res.*, 102, 19 383–19 402.
- 579 Chepfer H., P. Minnis, D. Young, L. Nguyen, and R. F. Arduini, 2002: Retrieval of cirrus cloud ice crystal shapes using  
580 visible reflectances from dual-satellite measurements, *J. Geophys Res*; 107, 10.1029/2000JD000240.
- 581 Chepfer, H., S. Bony, D. Winker, M. Chiriaco, J.-L. Dufresne, and G. Sèze, 2008: Use of CALIPSO lidar observations to  
582 evaluate the cloudiness simulated by a climate model, *Geophys. Res. Lett.*, 35, L15704, doi:10.1029/2008GL034207.

583 Chepfer, H., S. Bony, D. Winker, G. Cesana, J.-L. Dufresne, P. Minnis, C. J. Stubenrauch, and S. Zeng, 2010: The GCM-  
584 Oriented CALIPSO Cloud Product (CALIPSO-GOCCP), *J. Geophys. Res.*, 115, D00H16,  
585 doi:10.1029/2009JD012251

586 De Haan J., P. B. Bosma, and J. W. Hovenier, 1986: The adding method for multiple scattering of polarized light, *Astron.*  
587 *Astrophys.*, 183, 371-391.

588 Deschamps, P.-Y., F.-M. Bréon, M. Leroy, A. Podaire, A. Brickaud, J.-C. Buriez, and G. Sèze, 1994 : « The POLDER  
589 Mission : Instrument Characteristics and Scientific Objectives », *IEEE*, 32, 598-615.

590 Dufresne J.-L., and S. Bony, 2008: An assessment of the primary sources of spread of global warming estimates from  
591 coupled atmosphere-ocean models. *J. Climate*, 21(19), 5135-5144, doi: 10.1175/2008JCLI2239.1.

592 Dufresne J.-L. et al., 2013: Climate change projections using the IPSL-CM5 Earth System Model: from CMIP3 to CMIP5.  
593 *Clim. Dynamics*, 40(9-10), 2123-2165, doi: 10.1007/s00382-012-1636-1

594 Emanuel, K. A., 1991: A scheme for representing cumulus convection in large-scale models, *J. Atmos. Sci.*, 48, 2313–2335.

595 Fougnie, B., G. Bracco, B. Lafrance, C. Ruffel, O. Hagolle, and C. Tinel, 2007 : PARASOL in-flight calibration and  
596 performance, *Appl. Opt.*, 46, 5435–5451.

597 Grandpeix, J.-Y. and J.-P. Lafore, 2010: A density current parametrization coupled with Emanuel's convection scheme. Part  
598 I: The models, *J. Atmos. Sci.*, 67, 881-897.

599 Hale G. M. and M. R. Query, 1973: Optical constants of water in the 200nm to 200mm wavelength region, *Appl. Opt.*, 12,  
600 555-63.

601 Haynes, J.M., R.T. Marchand, Z. Luo, A. Bodas-Salcedo and G.L. Stephens, 2007: A Multipurpose Radar Simulation  
602 Package: QuickBeam, *Bull. Amer. Met. Soc.*, 88, 1723-1727.

603 Hourdin, F., I. Mousat, S. Bony, P. Braconnot, F. Cordon, J.-L. Dufresne, L. Fairhead, M.-A. Filiberti, P. Friedlingstein, J.-Y.  
604 Grandpeix, G. Krinner, P. Le Van, Z.-X. Li and F. Lott, 2006: The LMDZ general circulation model: climate  
605 performance and sensitivity to parameterized physics with emphasis on tropical convection. *Climate Dynamics*, 19  
606 (15), 3445-3482, DOI: 10.1007/s00382-006-0158-0.

607 Hourdin F., M.A. Foujols, F. Codron, V. Guemas, J.-L. Dufresne, S. Bony, S. Denvil, L. Guez, F. Lott, J. Gattas, P.  
608 Braconnot, O. Marti, Y. Meurdesoif and L. Bopp (2013-a): From LMDZ4 to LMDZ5 : impact of the atmospheric  
609 model grid configuration on the climate and sensitivity of IPSL climate model, *Climate Dynamics*, 40(9-10), 2167-  
610 2192, doi: 10.1007/s00382-012-1411-3

611 Hourdin F., J.-Y. Grandpeix, C. Rio, S. Bony, A. Jam, F. Cheruy, N. Rochetin, L. Fairhead, A. Idelkadi, I. Musat, J.-L.  
612 Dufresne, M.-P. Lefebvre, A. Lahellec and R. Roehrig (2013-b): From LMDZ5A to LMDZ5B : revisiting the

613 parameterizations of clouds and convection in the atmospheric component of the IPSL-CM5 climate model, *Climate*  
614 *Dynamics*, 40(9-10), 2193-2222, doi: 10.1007/s00382-012-1343-y.

615 Jakob, C., and G. Tselioudis, 2003: Objective identification of cloud regimes in the Tropical Western Pacific, *Geophys. Res.*  
616 *Letts.*, 30(21), 2082, doi:10.1029/2003GL018367.

617 Jam A, F. Hourdin, C. Rio and F. Couvreux, 2011: Resolved versus parametrized boundary-layer plumes. part iii: A  
618 diagnostic boundary-layer cloud parameterization derived from large eddy simulations, B.L.M. , submitted

619 Kawai H and Texeira, J. 2012. Probability density functions of liquid water path and total water content of marine boundary  
620 layer clouds: implications for cloud parameterization, *J. Climate*, 25, 2162-2177, DOI: 10.1175/JCLI-D-11-00117.1

621 Klein, S.A., and C. Jacob, 1999: Validation and sensitivities of frontal clouds simulated by the ECMWF model. *Mon.*  
622 *Weather Rev.*, 127, 2514-2531.

623 Klein, S.A., Y. Zhang, M.D. Zelinka, R. Pincus, J. Boyle, and P. J. Gleckler (2013), Are climate model simulations of clouds  
624 improving? An evaluation using the ISCCP simulator, *J. Geophys. Res. Atmos.*, 118, 1329–1342,  
625 doi:10.1002/jgrd.50141.

626 Konsta, D., H. Chepfer, and J.-L. Dufresne, 2012: A process oriented representation of tropical oceanic clouds for climate  
627 model evaluation, based on a statistical analysis of daytime A-train high spatial resolution observations, *Climate*  
628 *Dynamics*, 39(9-10), 2091-2108, doi:10.1007/s00382-012-1533-7

629 Li J, Dobbie S, Raisanen P, Min Q. 2005. Accounting for unresolved clouds in a 1-D solar radiative transfer model. *Q. J.*  
630 *Roy. Meteorol. Soc.* 131: 1607-1629.

631 Liu, Z., A. Omar, M. Vaughan, J. Hair, C. Kittaka, Y. Hu, K. Powell, C. Trepte, D. Winker, C. Hostetler, R. Ferrare, and R.  
632 Pierce, 2008: CALIPSO lidar observations of the optical properties of Saharan dust: A case study of long-range  
633 transport, *J. Geophys. Res.*, 113, D07207, doi:10.1029/2007JD008878.

634 Loeb N. G., B. A. Wielicki, D. R. Doelling, G. L. Smith, D. F. Keyes, S. Kato, N. Manalo-Smith and T. Wong, 2009:  
635 Toward Optimal Closure of the Earth's Top-of-Atmosphere Radiation Budget. *J. Climate*, 22(3), 748-766, doi:  
636 10.1175/2008JCLI2637.1

637 Mace G. G. and F. J. Wrenn, 2013: Evaluation of the Hydrometeor Layers in the East and West Pacific within ISCCP  
638 Cloud-Top Pressure-Optical Depth Bins Using Merged CloudSat and CALIPSO Data. *J. Climate*, 26, 9429-9444.

639 Marchand R., J. Haynes, G.G. Mace, T. Ackerman, and G. Stephens, 2009: A comparison of simulated cloud radar output  
640 from the multiscale modeling framework global climate model with CloudSat cloud radar observations. *J. Geophys.*  
641 *Res.*, 114, D00A20, doi:10.1029/2008JD009790.

642 Marti, O., P. Braconnot, J.-L. Dufresne, J. Bellier, R. Benshila, S. Bony, A. Caudel, F. Cordon, N. de Noblet, S. Denvil, L.

643 Fairhead, T. Fichet, M.-A. Foujols, P. Friedlingstein, H. goosse, J.-Y. Grandpeix, E. Guilyardi, F. Hourdin, A.  
644 Idelkadi, M. Kageyama, G. Krinner, C. Levy, G. Madec, J. Mignot, I. Musat, D. Swingedow, C. Talandier, 2010: Key  
645 features of the IPSL ocean atmosphere model and its sensitivity to atmospheric resolution, *Clim. Dyn.*, 34, 1-26.

646 Martins, E., V. Noel, and H. Chepfer, 2011: Properties of cirrus and subvisible cirrus from CALIOP, related to atmospheric  
647 dynamics and water vapor, *J. Geophys. Res.*, 116, D02208.

648 Medeiros, B., L. Nuijens, C. Antoniazzi, and B. Stevens, 2010: Low-latitude boundary layer clouds as seen by CALIPSO, *J.*  
649 *Geophys. Res.*, 115, D23207, doi:10.1029/2010JD014437

650 Medeiros, B., and B. Stevens, 2011: Revealing differences in GCM representations of low clouds, *Clim. Dyn.*, 36,385-399

651 Minnis, P., W. L. Jr. Smith, D. P. Garber, J. K. Ayers, and D. R. Doelling, 1955: Cloud Properties Derived from GOES-7 for  
652 the Spring 1994 ARM Intensive Observing Period Using Version 1.0.0 of the ARM Satellite Data Analysis Program.  
653 NASA RP 1366, 59.

654 Nam, C.; Bony, S.; Dufresne, J.-L.; Chepfer, H., 2012; The "too few, too bright" tropical low-cloud problem in CMIP5  
655 models. *Geophys. Res. Lett.*, 39(21), L21801, doi: 10.1029/2012GL053421

656 Noel, V., A. Hertzog, H. Chepfer, and D. M. Winker, 2008: Polar stratospheric clouds over Antarctica from the CALIOP  
657 spaceborn lidar, *J. Geophys. Res.*, 113, D02205, doi:10.1029/2007JD008616

658 Noel, V. and H. Chepfer, 2010: A global view of horizontally-oriented crystals in ice clouds from CALIPSO, *J. Geophys.*  
659 *Res.*, 115, D012365.

660 Parol F., J.C. Buriez, C. Vanbauce, J. Riedi, L. C.-Labonnote, M. Doutriaux-Boucher, M. Vesperini, G. Sèze, P. Couvert, M.  
661 Viollier, F.M. Bréon , 2004 : Capabilities of multi-angle polarization cloud measurements from satellite: POLDER  
662 results, *Adv. Space Res.* , 33, 1080-1088

663 Pincus R, Klein SA., 2000. Unresolved spatial variability and microphysical process rates in large-scale models. *J. Geophys.*  
664 *Res.* 105(D22): 27059-27065.

665 Pitts, M.C., L.W. Thomason, L.R. Poole, and D.M. Winker, 2007: Characterization of Polar Stratospheric Clouds with  
666 Space-Borne Lidar: CALIPSO and the 2006 Antarctic Season, *Atmos. Chem. Phys. Discuss.*, 7, 7933-7985.

667 Randall, D. A., R. A. Wood, S. Bony, R. Colman, T. Fichet, J. Fyfe, V. Kattsov, A. Pitman, J. Shukla, J. Srinivasan, R. J.  
668 Stouffer, A. Sumi and K. E. Taylor, 2007 : Climate Models and Their Evaluation. In: *Climate Change 2007: The*  
669 *Physical Science Basis. Contribution of Working Group I to the Fourth Assessment Report of the Intergovernmental*  
670 *Panel of Climate Change* [Solomon, S., D. Qin, M. Manning, Z. Chen, M. Marquis, K. B. Averyt, M. Tignor and H.L.  
671 Miller (eds.)]. Cambridge University Press, Cambridge, United Kingdom and New York, NY, USA.

672 Rio, C., J-Y Grandpeix, F. Hourdin, F. Guichard, F. Couvreur, J-P Lafore, A. Fridlind, A. Mrowiec, R. Roehrig, N.

673 Rochetin, M.-P. Lefebvre, A. Idelkadi (2013). Control of deep convection by sub-cloud lifting processes: the ALP  
674 closure in the LMDZ5B general circulation model; *Climate Dynamics*, 40, 2271-2292, doi:10.1007/s00382-012-1506-  
675 x

676 Rio, C. and F. Hourdin, 2008: A Thermal Plume Model for the Convective Boundary Layer: Representation of Cumulus  
677 Clouds, *J. Atmos. Sci.*, 65, 407-425.

678 Rio, C., F. Hourdin, F. Couvreux and A. Jam, 2010: Resolved Versus Parametrized Boundary-Layer Plumes. Part II:  
679 Continuous Formulations of Mixing Rates for Mass-Flux Schemes. *Boundary-layer Meteorol* 135:469–483,  
680 10.1007/s10546-010-9478-z

681 Rossow, W. B., and R. A. Schiffer, 1991: ISCCP cloud data products, *Bull. Amer. Meteorol. Soc.*, 72, 2 – 20.

682 Rossow, W. B., G. Tselioudis, A. Polak, and C. Jakob, 2005: Tropical climate described as a distribution of weather states  
683 indicated by distinct mesoscale cloud property mixtures, *Geophys. Res. Lett.*, 32, L21812,  
684 doi:10.1029/2005GL024584.

685 Sassen K., Z. Wang, and D. Liu, 2008: Global distribution of cirrus clouds from CloudSat/Cloud-Aerosol Lidar and Infrared  
686 Pathfinder Satellite Observations (CALIPSO) measurements, *J. Geophys. Res.*, 113, D00A12,  
687 doi:10.1029/2008JD009972.

688 Siebesma A.P., C.S. Bretherton, A. Brown, A. Chlond, J. Cuxart, P.G. Duynkerke H. Jiang, M. Khairoutdinov, D. Lewellen,  
689 C-H. Moeng, E. Sanchez, B. Stevens and D.E. Stevens, 2003: A Large-Eddy Simulation intercomparison study of  
690 shallow cumulus convection, *J. Atmos. Sci.* 60 1201-1219

691 Simmons A., S. Uppala, D. Dee, S. Kobayashi, 2007: ERA-interim: new ECMWF reanalysis products from 1989 onwards,  
692 *ECMWF Newsl.*, 110, 29-35

693 Soden B. J. and I. M. Held, 2006: An assessment of climate feedbacks in coupled ocean-atmosphere models. *J. Climate*,  
694 19, 3354-3360.

695 Stubenrauch C, W. Rossow, S. Kinne, 2012: Assessment of Global Cloud Data Sets from Satellites, A Project of the World  
696 Climate Research Programme Global Energy and Water Cycle Experiment (GEWEX) Radiation Panel, WCRP Report  
697 No. 23/2012

698 Vial, J. , J-L Dufresne, S. Bony, 2013. On the interpretation of inter-model spread in CMIP5 climate sensitivity estimates;  
699 *Clim. Dynamics*, 41, 3339-3362, doi: 10.1007/s00382-013-1725-9

700 Vuolo R.M., H. Chepfer, L. Menut, and G. Cesana, 2009: Comparison of mineral dust layers vertical structures modeled  
701 with CHIMERE-DUST and observed with the CALIOP lidar, *J. Geophys. Res.*, 114, D09214,  
702 doi:10.1029/2008JD011219.

703 Warren S. G. , 1984: Optical constants of ice from the ultraviolet to the microwave., *Appl. Opt.*, 23, 1206-25.

704 Webb M., C. Senior, S. Bony and J.-J. Morcrette, 2001: Combining ERBE and ISCCP data to assess clouds in three climate  
705 models, *Climate Dynamics*, 17, 905-922.

706 Webb, M. J., C. A. Senior, D. M. H. Sexton, W. J. Ingram, K. D. Williams, M. A. Ringer, B. J. McAvaney, R. Colman, B. J.  
707 Soden, R. Gudgel, T. Knutson, S. Emori, T. Ogura, Y. Tsushima, N. G. Andronova, B. Li, I. Musat, S. Bony, and K. E.  
708 Taylor, 2006: On the contribution of local feedback mechanisms to the range of climate sensitivity in the two GCM  
709 ensembles. *Clim. Dyn.*, 27, 17-38, doi: 10.1007/s00382-006-0111-2.

710 Williams, K. D., and G. Tselioudis, 2007: GCM intercomparison of global cloud regimes: present-day evaluation and  
711 climate change response. *Clim. Dyn.*, 29, 231-250, doi: 10.1007/s00382-007-0232-2.

712 Winker D., W. Hunt, and M. McGill, 2007: Initial Performance Assessment of CALIOP, *Geophys. Res. Lett.*, 34, L19803,  
713 doi:10.1029/2007GL030135.

714 Yang P., K. N. Liou, K. Wyser, D. Mitchell, 2000: Parameterization of the scattering and absorption properties of individual  
715 ice crystals., *J. Geophys. Res.*, 105, 4699-4718.

716 Yang P., B-C. Gao, B. A. Baum, W. J. Wiscombe, Y. X. Hu, S. L. Nasiri, P. F. Soulen, A. J. Heymsfield, G. M., Mc Farquhar,  
717 and L. M. Miloshevich, 2001: Sensitivity of cirrus bidirectional reflectance to vertical inhomogeneity of ice crystal  
718 habits and size distributions for two Moderate-Resolution Imaging Spectroradiometer (MODIS) bands , *J. Geophys.*  
719 *Res*, 106, 17267-17291.

720 Yu W., M. Doutriaux, G. Seze, H. Le Treut, and M. Desbois, 1996: A methodology study of the validation of clouds in  
721 GCMs using ISCCP satellite observations. *Clim. Dyn.*, 12: 389-401.

722 Zhang M H, W.Y. Lin, S.A. Klein, J.T. Bacmeister, S.Bony, R.T. Cederwall, A.D. Del Genio, J.J. Hack, N.G. Loeb, U.  
723 Lohmann, P. Minnis, I. Musat, R. Pincus, P. Stier, M.J. Webb, J.J.B. Wu, S.C. Xie, M.-S. Yao, and J.H. Zhang, 2005:  
724 Comparing Clouds And Their Seasonal Variations in 10 Atmospheric General Circulation Models With Satellite  
725 Measurements, *J. Geophys. Res.*, 110, D15S02, doi:10.1029/2004JD005021.

726 Zhang Y., S.A. Klein, J. Boyle, and G.G. Mace, 2010: Evaluation of tropical cloud and precipitation statistics of Community  
727 Atmosphere Model version 3 using CloudSat and CALIPSO data. *J. Geophys. Res.*, 115, D12205,  
728 doi:10.1029/2009JD012006.

729

730

731

732 **Annex**

733

## 734 **Annex A: Spatio-temporal sampling of CALIPSO and PARASOL observations**

735

736 (i) Temporal resolution:

737 The two instruments follow the same sun-synchronous A-train orbit, which passes over each location twice a day at about  
738 1:30 AM and 1:30 PM local solar time. As PARASOL collects measurements during daytime, only the daytime CALIPSO  
739 data are considered. The two instruments fly over the same orbit so they document the same cloud parcel simultaneously at  
740 about 1:30 AM local solar time.

741 The incomplete sampling of the diurnal cycle has negligible impact (less than 1%) on the results [Chepfer et al., 2008].

742

743 (ii) Spatial resolution

744 As a PARASOL pixel (6x6km) is much larger than a CALIOP/CALIPSO one (330m along-track, 75m cross-track), one  
745 value of the directional reflectance is associated to at least 18 lidar profiles. To overcome these differences, the CALIOP  
746 cloud cover and the PARASOL reflectance are processed independently on a statistical basis and then compared to daily  
747 mean values on a  $2^\circ \times 2^\circ$  grid (several hundreds of  $\text{km}^2$ ). To test the impact of the sampling over seasonal mean results on a  
748  $2^\circ \times 2^\circ$  grid, two PARASOL reflectance datasets were built in the same viewing direction ( $\theta_v = 27^\circ, \phi_s - \phi_v = 320^\circ$ ): the first  
749 dataset includes all reflectance values measured by PARASOL, and the second dataset includes only the reflectance  
750 measured along the CALIPSO ground track. The maximum distance between a PARASOL and a CALIOP pixel in the first  
751 dataset is 50km. The number of measurements is about 30% lower in the second dataset. Maps of  $2^\circ \times 2^\circ$  mean directional  
752 reflectances and variances (not shown) are similar for both datasets although the second one is noisier, thus suggesting that  
753 both PARASOL datasets (collocated or not with CALIOP) can be analyzed. The similarity between the two datasets also  
754 shows that the few PARASOL pixels collocated with CALIOP (6x6  $\text{km}^2$ ) are representative of all PARASOL pixels  
755 included in the  $2^\circ \times 2^\circ$  grid cell.

756 Similarly, it is thus reasonable to consider that the CALIOP dataset (even with a 330mx75m resolution) when averaged over  
757 several months is statistically representative of the monthly/seasonal cloud cover within a GCM grid cell.

758

759

760

761

## 762 **Annex B: Sensitivity of the PARASOL monodirectional reflectance to the** 763 **atmosphere's composition**

764

### 765 *(i) Optical properties*

766 The cloud particle optical properties (e.g. single scattering albedo, scattering phase function, extinction coefficient) depend  
767 on the wavelength, the particle size and its shape. As the absorption phenomena is negligible in both ice and water at 864nm  
768 [Warren et al 1984 ; Hale and Querry, 1973], the single scattering albedo is close to one regardless of the size and shape of  
769 the particles. As the radius of cloud particles are always larger than the wavelength considered here, the scattering phase  
770 function is not very sensitive to the droplet size but it is sensitive to the particle shape. A spherical shape assumption, which  
771 is typical of liquid water computed with the Mie theory and a non-spherical shape, which is typical [Chepfer et al. 2002] of  
772 ice crystals whose optical properties are computed with Geometric Optic enhanced with Finite Differential Time Domain  
773 [Yang et al 2000 and 2001] are used. As shown in Fig. C.a, their scattering phase functions differ significantly for scattering  
774 angles close to backscattering ( $180^\circ$ ), haloes ( $22^\circ$  and  $44^\circ$ ) and rainbow ( $140^\circ$ ), and also between  $90^\circ$  and  $130^\circ$ , which  
775 corresponds to the viewing and solar zenith angle selected for PARASOL data in the Tropics. Complementary computations  
776 (not shown) indicate that the scattering phase function (at this wavelength) weakly depends on the particle size compared to  
777 the influence of the shape. On the contrary, the particle extinction coefficient is directly dependent on the particle size: it is  
778 proportional to the scattering efficiency (close to 2 as the particles are large than the wavelength) multiplied by the particle  
779 cross section, which is expressed as the function of the particle size.

780

### 781 *(ii) Radiative transfer computations*

782 The directional reflectance is computed using a doubling-adding radiative transfer code [DeHaan et al. 1986]. The cloud  
783 particles optical properties such as the single scattering albedo and the truncated scattering phase function developed in  
784 Legendre polynomial are introduced in the radiative transfer code. The Rayleigh scattering is also taken into account in the  
785 computation even though its contribution to the total directional reflectance remains small ( $\tau$  is about 0.013 for the whole  
786 atmospheric column). As the studied viewing direction is off-glitter, the ocean is described as a Lambertian surface with a  
787 constant plane albedo of 0.03. The directional reflectance is then computed as in Chepfer et al. [2002] for various cloud  
788 optical depths and solar zenith angles.

789 Figure C.b shows that changes of reflectance values due to solar zenith angle variations are less than 0.1 in the tropical  
790 regions ( $30^\circ\text{S}-30^\circ\text{N}$ ,  $18^\circ < \theta_s < 60^\circ$ ) for a given phase function. It reaches a maximum of 0.15 between the ITCZ and the

791 higher observable latitudes ( $\theta_s > 60^\circ$ ). Thus variations of the latitudinal reflectance larger than 0.15 (0.1 in the Tropics)  
792 cannot be attributed to variations of  $\theta_s$ . They are due to changes in the atmosphere composition (clouds). The sensitivity of  
793 the reflectance to the cloud particles scattering phase function is maximum at high latitudes / high solar zenith angle (0.13)  
794 and slightly reduces in the tropics (0.1).

795

796 (iii) *PARASOL simulator*

797

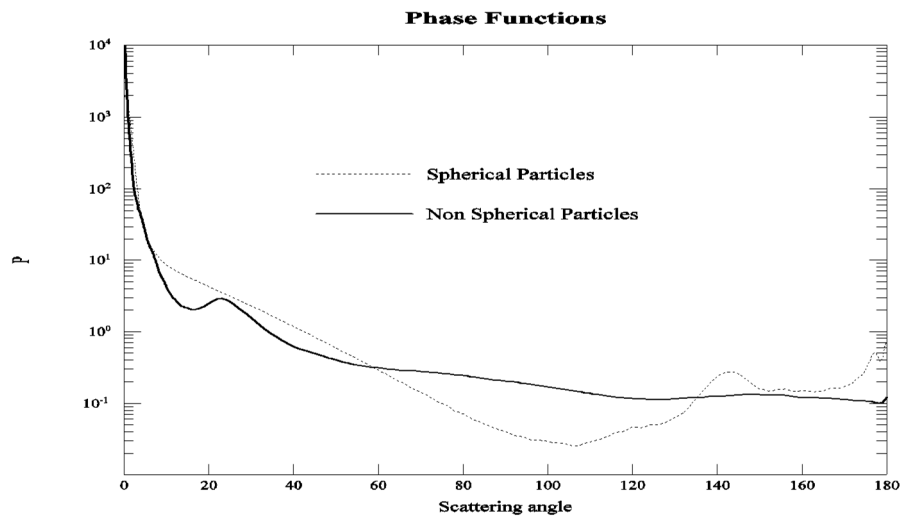
798 The PARASOL simulator is initiated with the mixing ratios of in-cloud liquid and ice water content in each model grid cell  
799 that are then converted into sub-grid mixing ratios using SCOPS. In each subcolumn, the total cloud optical depth ( $\tau_{tot}$ )  
800 is the sum of the subcolumn ice ( $\tau_{tot\_ice}$ ) and liquid ( $\tau_{tot\_liq}$ ). These are computed assuming that the cloud particles  
801 are spherical with a radius equal to the effective radius predicted by the model. For five solar zenith angles ( $\theta_s = 0^\circ, 20^\circ,$   
802  $40^\circ, 60^\circ$  and  $80^\circ$ ) and knowing the total cloud optical depth, two directional reflectance values are then computed for  
803 each day and for each solar zenith angle assuming that the cloud is entirely composed of liquid water (Refl\_liq) or ice  
804 water (Refl\_ice). These reflectance values are derived from a bilinear interpolation over pre-calculated look-up tables  
805 containing results of radiative transfer computations (Annex B) for the cloud particle's shape assumption (spherical and  
806 non spherical) made in the model. The subgrid directional reflectance is then computed as follow:  $Refl =$   
807  $(Refl\_liq * \tau_{tot\_liq} + Refl\_ice * \tau_{tot\_ice}) / \tau_{tot}$ . The directional reflectance obtained for each subgrid is then averaged  
808 over each GCM grid cell for each day and for each  $\theta_s$ . After the simulations have been performed, the five  
809 monodirectional reflectances corresponding to the five solar zenith angles from the simulator's outputs are used to  
810 interpolate linearly the monodirectional reflectance depending on the monthly mean value of the solar zenith angle at  
811 each grid point. The simulated monodirectional reflectance is then directly comparable to the observations.

812 **Figure B:**

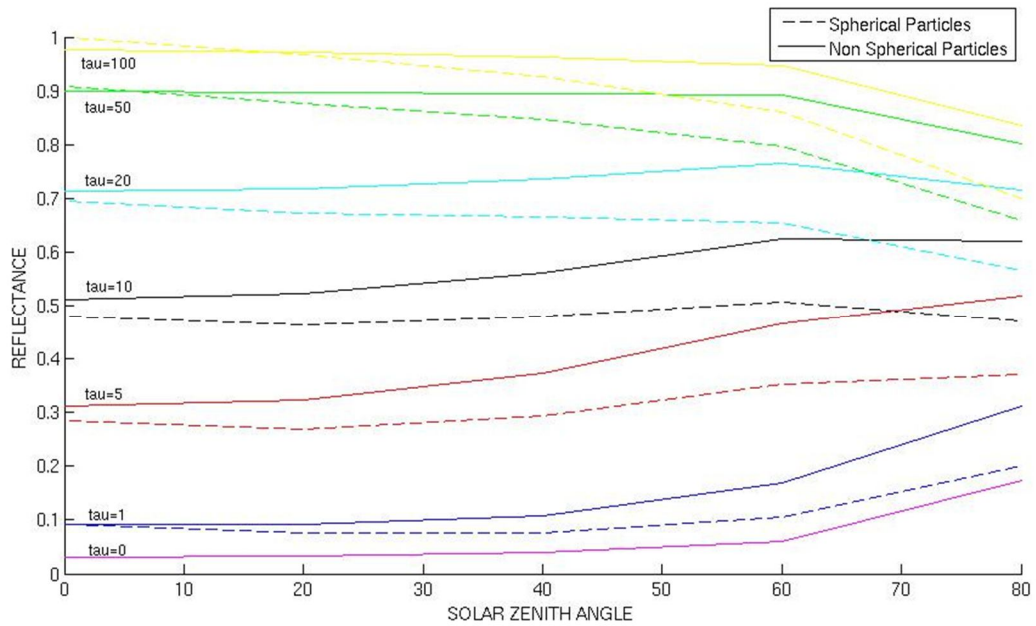
813 a) Scattering phase function for spherical and non-spherical particles. Monodirectional reflectance simulated as a  
814 function of the solar zenith angle for spherical and non-spherical particles in the viewing direction ( $\theta_v = 27^\circ \phi_v = 320^\circ$ ).

815

816



817  
818  
819  
820  
821  
822



823  
824  
825  
826

827

828

829

830

831

832

833

834

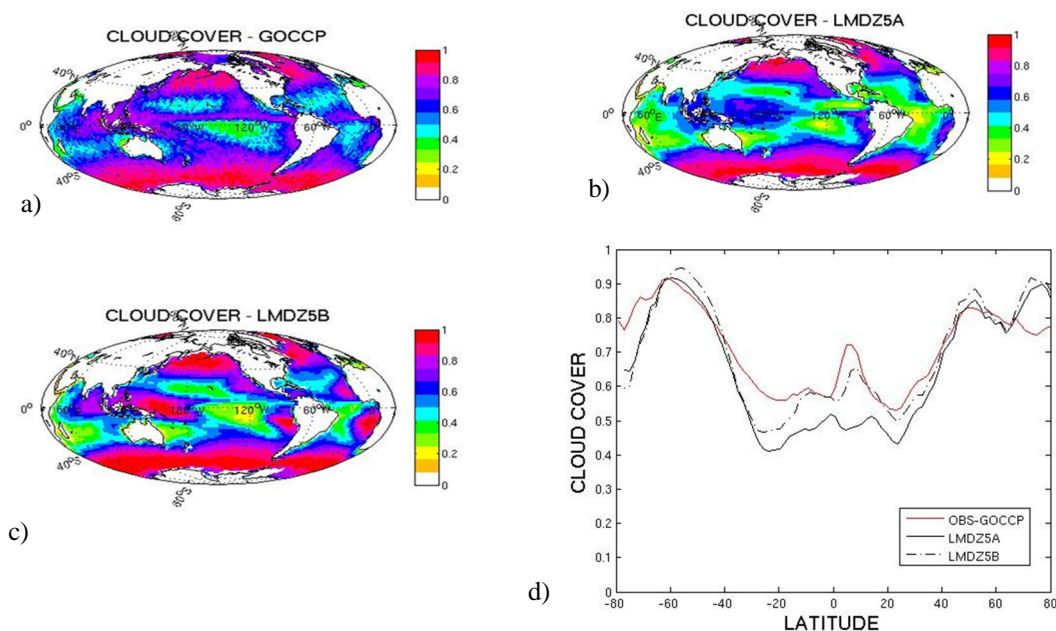
835

## 836 Annex C: Traditional global monthly mean evaluation of cloud properties

837 a) Cloud cover

838 On average, cloud cover is underestimated over the tropical regions and is broadly consistent with observations in the mid  
839 and high latitudes (Fig. C1). In the Tropical Western Pacific, along the ITCZ and the SPCZ, the cloud cover simulated by  
840 LMDZ5A is about 60-70% whereas observations indicate a cloud cover ranging from 80% to 100%. In regions where the  
841 cloud cover is low, such as in the trade wind cumulus region, observations indicate a cloud fraction between 40 and 60%  
842 whereas the simulated cloud cover is only about 20 to 50%. Although LMDZ5B underestimates the averaged cloud cover in  
843 the tropics, the bias is reduced by a factor close to 2 compared to LMDZ5A. The improvement is very significant in almost  
844 all fully overcast regions (e.g. warm-pool, east Pacific and Atlantic) and even with an overestimated cloud cover.

**Figure C1 :** Geographical distribution of the total mean cloud cover over the ocean averaged over the period 2007-2008 (a) observed with CALIPSO-GOCCP during day time, (b) simulated with LMDZ5A and the lidar simulator, (c) simulated with LMDZ5B and the lidar simulator; (d) zonal mean of the same quantity observed (red line) and simulated (LMDZ5A: black line and LMDZ5B: black dotted line).



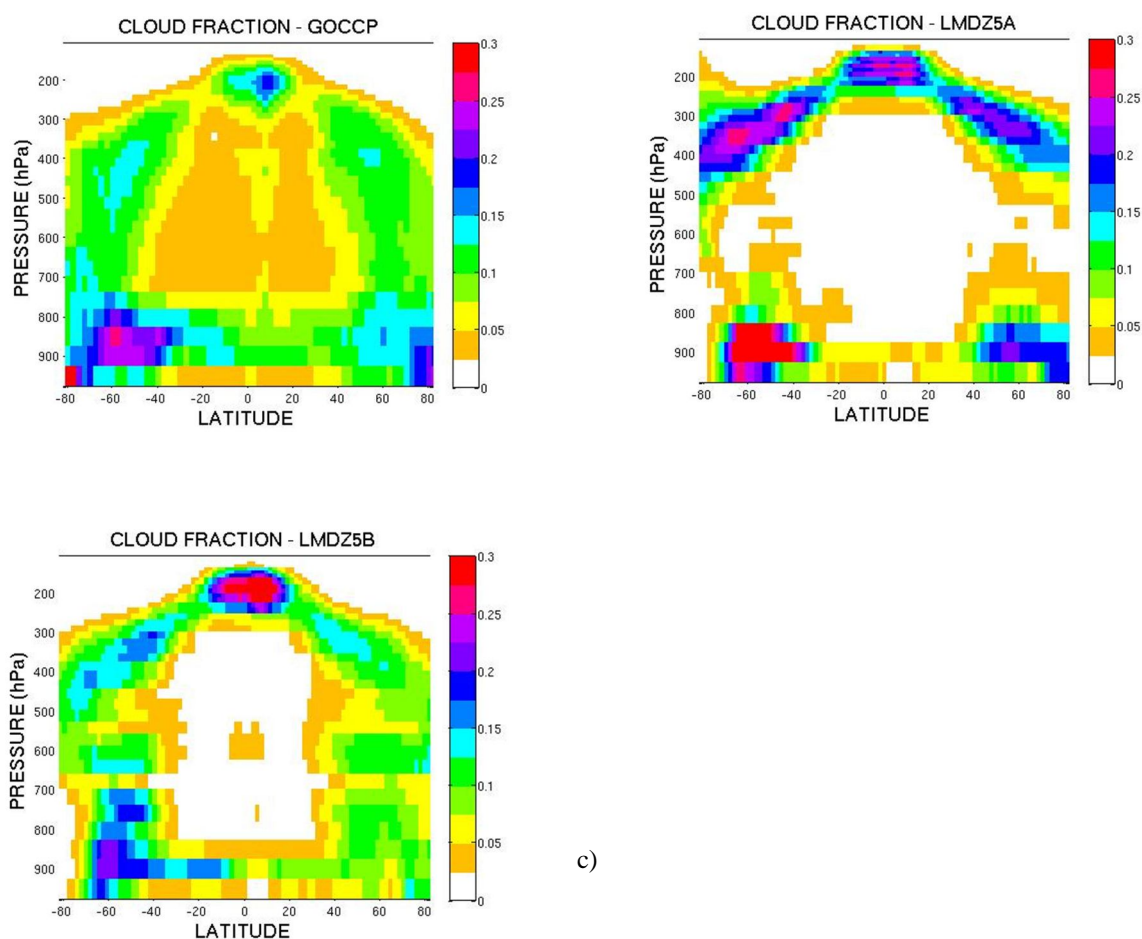
845

846 b) Cloud vertical profile

847 The zonal mean vertical distribution of the observed CALIPSO-GOCCP cloud fraction clearly highlights the well-known  
848 links between cloud characteristics and large circulation of the atmosphere (Fig. C2-a). The altitude of the higher clouds  
849 follows the tropopause height and decreases from the equator to the poles. The LMDZ5A model with the lidar simulator  
850 produces a cloud fraction of high-level clouds that is too large almost everywhere and the altitude of these clouds is too  
851 high, in particular over the polar region in the southern hemisphere (Fig. C2-b). In the tropics, LMDZ5A strongly

852 underestimates the cloud fraction at low and middle altitudes. Although this feature is amplified by the masking effect of  
 853 high clouds on the lidar signal (thick high level clouds, with typical  $C\tau > 3$ , attenuate the signal and mask low- and mid-level  
 854 clouds that might exist below them), this underestimation already occurs with the cloud cover simulated by the model (i.e.  
 855 without using the lidar simulator, cf Chepfer et al., 2008). At higher latitudes, the model cannot simulate the large vertical  
 856 extent of the frontal clouds associated with storms. Instead, it simulates two separate groups of low- and high-level clouds.  
 857 This zonal mean vertical distribution of clouds is improved in LMDZ5B (Fig. C2-c). In the tropics, boundary level clouds  
 858 are present although they are too low and too concentrated in one single layer. At middle and high latitudes, the model  
 859 almost simulates the continuous vertical structure of the cloud fraction.

**Figure C2:** Zonal mean cloud fraction profile averaged over the period 2007-2008, a) observed from CALIPSO-GOCCP, b) simulated with LMDZ5A and the lidar simulator and c) simulated with LMDZ5B and the lidar simulator.



a)

b)

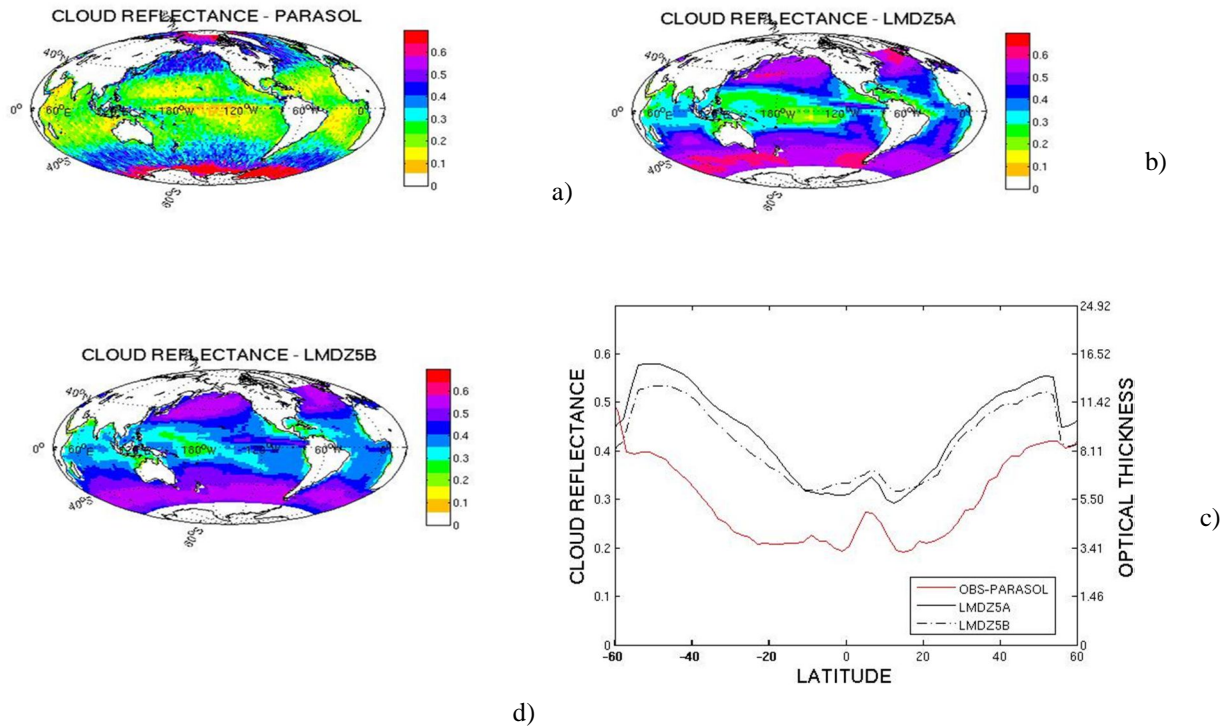
c)

### c) Cloud reflectance

In the trade wind regions, the observed cloud reflectance (typical value of 0.15) is only slightly higher than the clear-sky value (approximately 0.03), indicating that clouds are optically thin. This is not the case for the two model versions (Figure C3-b,c). They strongly overestimate the cloud reflectance almost everywhere, in particular over the subtropical oceans and

in the mid and high latitudes. The models cannot reproduce the contrast between the higher values ( $\approx 0.3$ ) of cloud reflectance observed along the ITCZ and the Eastern Pacific ocean and the lower values ( $< 0.2$ ) over the tropical trade wind cumulus region. They simulate high cloud reflectances ( $> 0.2$ ) over the tropics. On average, the cloud reflectance, and therefore the cloud optical thickness, simulated by the models over the ocean is too high almost everywhere.

**Figure C3:** Same as Fig. C1 for the monodirectional cloud reflectance over ocean, on average for the period 2007-2008 (a) observed with PARASOL, (b) simulated with LMDZ5A and the PARASOL simulator, (c) simulated with LMDZ5B and the PARASOL simulator; (d) zonal mean of the same quantity observed (red line) and simulated (LMDZ5A: black line and LMDZ5B: black dotted line).



## 860 List of Figures

861 1. (a) Cloud cover, (b) cloud reflectance (approximative optical depth on the right y-axis, see Sect. 2.3), (c) SW

862 albedo as a function of the vertical velocity  $\omega_{500}$  and d) PDF of  $\omega_{500}$ , observed (coloured lines), simulated with LMDZ5A  
863 (black line), simulated with LMDZ5B (black dotted line). For the cloud cover and the cloud reflectance the simulator is  
864 used for model results. All the data are monthly means over the tropical oceans. The monthly mean vertical velocity are  
865 from the ERA interim reanalysis [Simmons et al. 2007] and the short wave planetary albedo is estimated from CERES -  
866 EBAF (Clouds and the Earth's Radiant Energy System) [Loeb et al. 2009].

867 2. Cloud top pressure versus optical thickness (PC-tau) histograms, computed over the tropical oceans (a,d) observed,  
868 (b,e) simulated with the LMDZ5A model and the simulator and (c,f) simulated with the LMDZ5B model and the simulator.  
869 The upper line (a,b,c) corresponds to CALIPSO-GOCCP and PARASOL data (2007-2008) and simulator and the lower line  
870 (d,e,f) corresponds to ISCCP-D2 data (1983-2007) and simulator respectively. The color bar represents the number of points  
871 at each grid cell (PC-tau) divided by the total number of points in the histogram.

3. 2D histograms of cloud reflectance and cloud cover over the tropical oceans (a,d) observed with PARASOL and  
CALIPSO GOCCP, (b,e) simulated with LMDZ5A and the simulator, and (c,f) simulated with LMDZ5B and the simulator.  
The upper line (a,b,c) corresponds to instantaneous values and the lower line (d,e,f) corresponds to monthly mean values.  
The color bar represents the number of points at each grid cell (cloud cover-cloud reflectance) divided by the total number  
of points.

4. (a) PDF of cloud reflectances and (b,c,d) vertical profile of the cloud fraction CF3D for three classes defined by the  
grid average cloud reflectance (b)  $CR < 0.2$ , (c)  $0.2 < CR < 0.5$ , (d)  $CR > 0.5$ . Red line corresponds to observed values from  
PARASOL and CALIPSO-GOCCP respectively, black line corresponds to simulated values with LMDZ5A and the  
simulator and black dotted line corresponds to simulated values with LMDZ5B and the simulator. The data are  
instantaneous values and are taken only over the tropical oceans.

5. Cumulated distribution function of the cloud cover for high level clouds (upper row) and average relationship  
between total cloud cover and the normalized cloud cover of high level cloud (lower row, see text) in ascent (left column)  
and subsidence (right column) regions, observed with CALIPSO-GOCCP (red line), simulated with LMDZ5A and the  
simulator (black line), and simulated with LMDZ5B and the simulator (black dotted line). The cloud cover are  
instantaneous values and the ascent and the subsidence regions are defined as regions over the tropical ocean where the  
monthly mean value of  $\omega_{500}$  is respectively negative and positive.

6. 2D histograms of instantaneous cloud reflectance and cloud cover over the tropical ocean for situations where low  
level clouds dominate ( $CC_{low} > 0.9 * CC$ ) (a, d) observed, (b, e) simulated with LMDZ5A and the simulator, and (c, f)  
simulated with LMDZ5B and the simulator. The upper line (a,b,c) corresponds to PARASOL observations, CALIPSO

observations and simulator respectively and the lower line (d,e,f) corresponds to ISCCP. The color bar represents the number of points at each grid cell (cloud cover-cloud reflectance) divided by the total number of points.

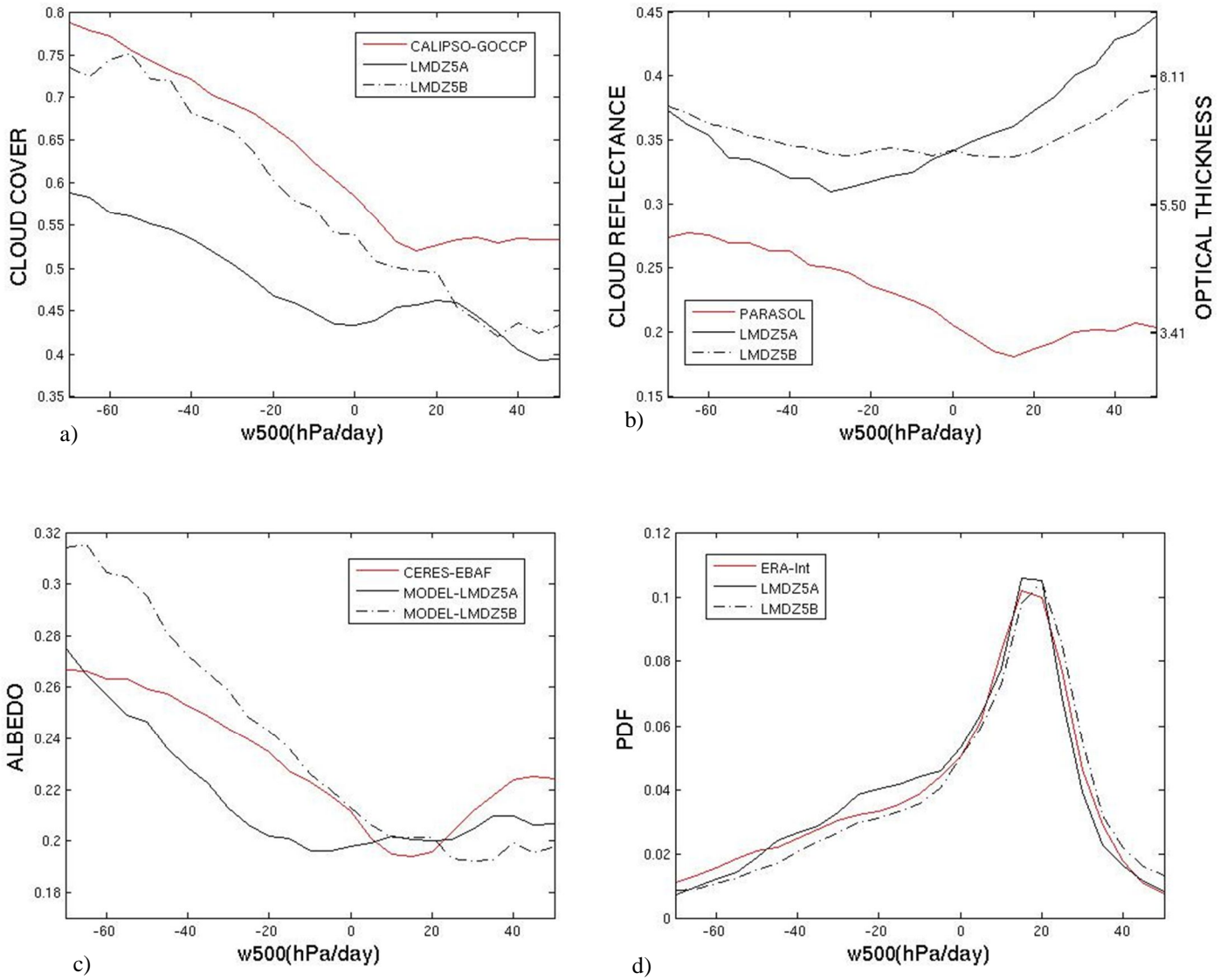
7. Instantaneous mean cloud reflectance as a function of cloud top pressure for mainly low-cloud situations (using the criterion:  $CC_{low} > 0.9 * CC$ ) over the tropical ocean, observed with PARASOL and CALIPSO-GOCCP (red line), simulated with LMDZ5A and the simulator (black line), and simulated with LMDZ5B and the simulator (black dotted line).

CTP is defined as the highest level of low clouds where the local cloud cover is greater than 0.1.

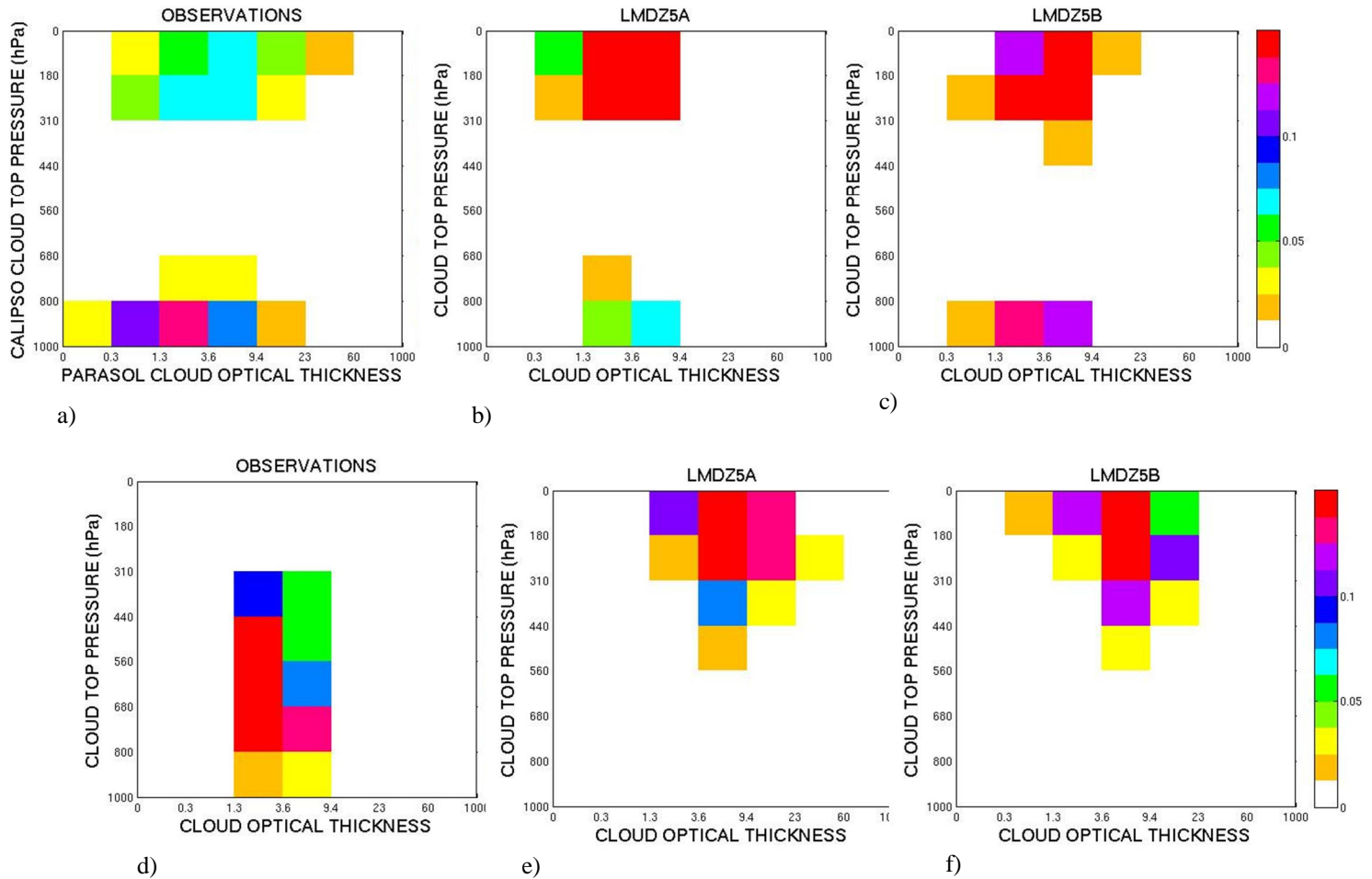
8. 2D histograms of instantaneous of (a) cloud liquid water path versus cloud reflectance simulated with LMDZ5A for conditions where low-level-clouds dominate ( $CC_{low} > 0.9 * CC$ ) (b) cloud reflectance versus cloud cover with the modified parameterization in LMDZ5A (see text) for all clouds and (c) for conditions where low-level-clouds dominate ( $CC_{low} > 0.9 * CC$ ). The color bar represents the number of points at each grid cell divided by the total number of points.

# Figures

**Figure 1:** (a) Cloud cover, (b) cloud reflectance (approximative optical depth on the right y-axis, see Sect. 2.3), (c) SW albedo as a function of the vertical velocity  $\omega_{500}$  and d) PDF of  $\omega_{500}$ , observed (coloured lines), simulated with LMDZ5A (black line), simulated with LMDZ5B (black dotted line). For the cloud cover and the cloud reflectance the simulator is used for model results. All the data are monthly means over the tropical oceans. The monthly mean vertical velocity are from the ERA interim reanalysis [Simmons et al. 2007] and the short wave planetary albedo is estimated from CERES - EBAF (Clouds and the Earth's Radiant Energy System) [Loeb et al. 2009].

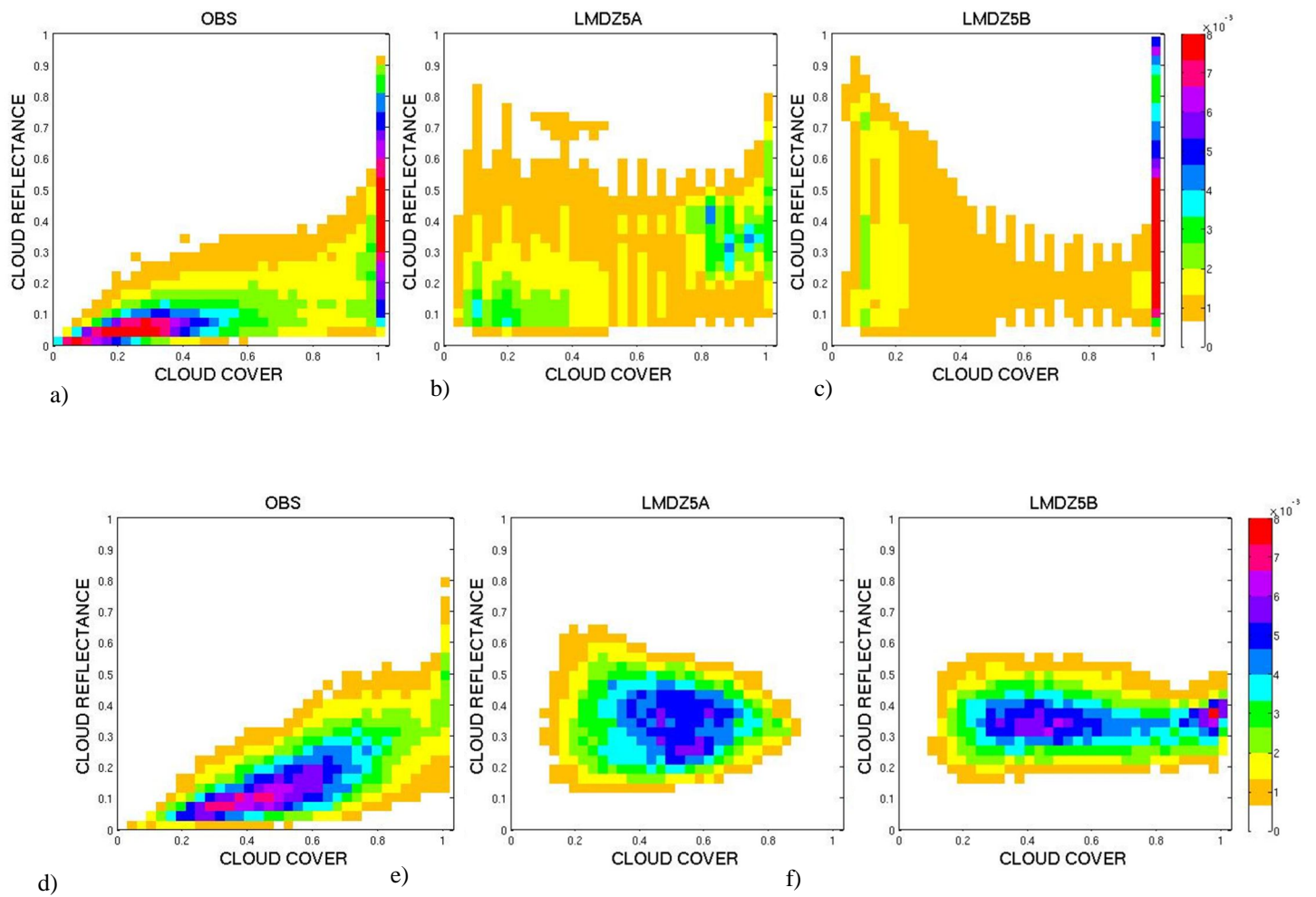


**Figure 2:** Cloud top pressure versus optical thickness (PC-tau) histograms, computed over the tropical oceans (a,d) observed, (b,e) simulated with the LMDZ5A model and the simulator and (c,f) simulated with the LMDZ5B model and the simulator. The upper line (a,b,c) corresponds to CALIPSO-GOCCP and PARASOL data (2007-2008) and simulator and the lower line (d,e,f) corresponds to ISCCP-D2 data (1983-2007) and simulator respectively. The color bar represents the number of points at each grid cell (PC-tau) divided by the total number of points in the histogram.

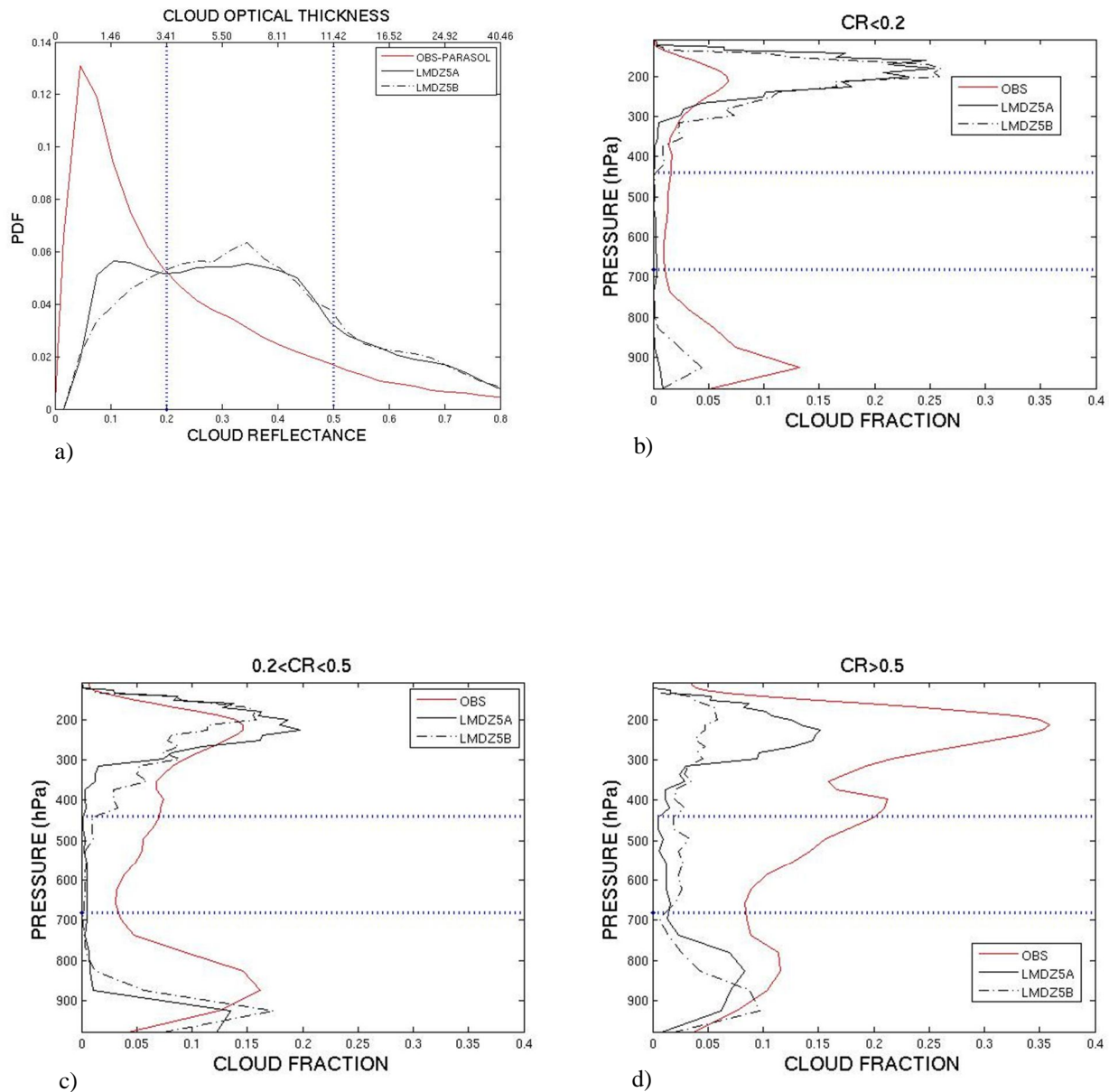


**Figure 3:** 2D histograms of cloud reflectance and cloud cover over the tropical oceans (a,d) observed with PARASOL and CALIPSO GOCCP, (b,e) simulated with LMDZ5A and the simulator, and (c,f) simulated with LMDZ5B and the simulator. The upper line (a,b,c) corresponds to instantaneous values and the lower line (d,e,f) corresponds to monthly mean values. The color bar represents the number of points at each grid cell (cloud cover-cloud reflectance) divided by the total number

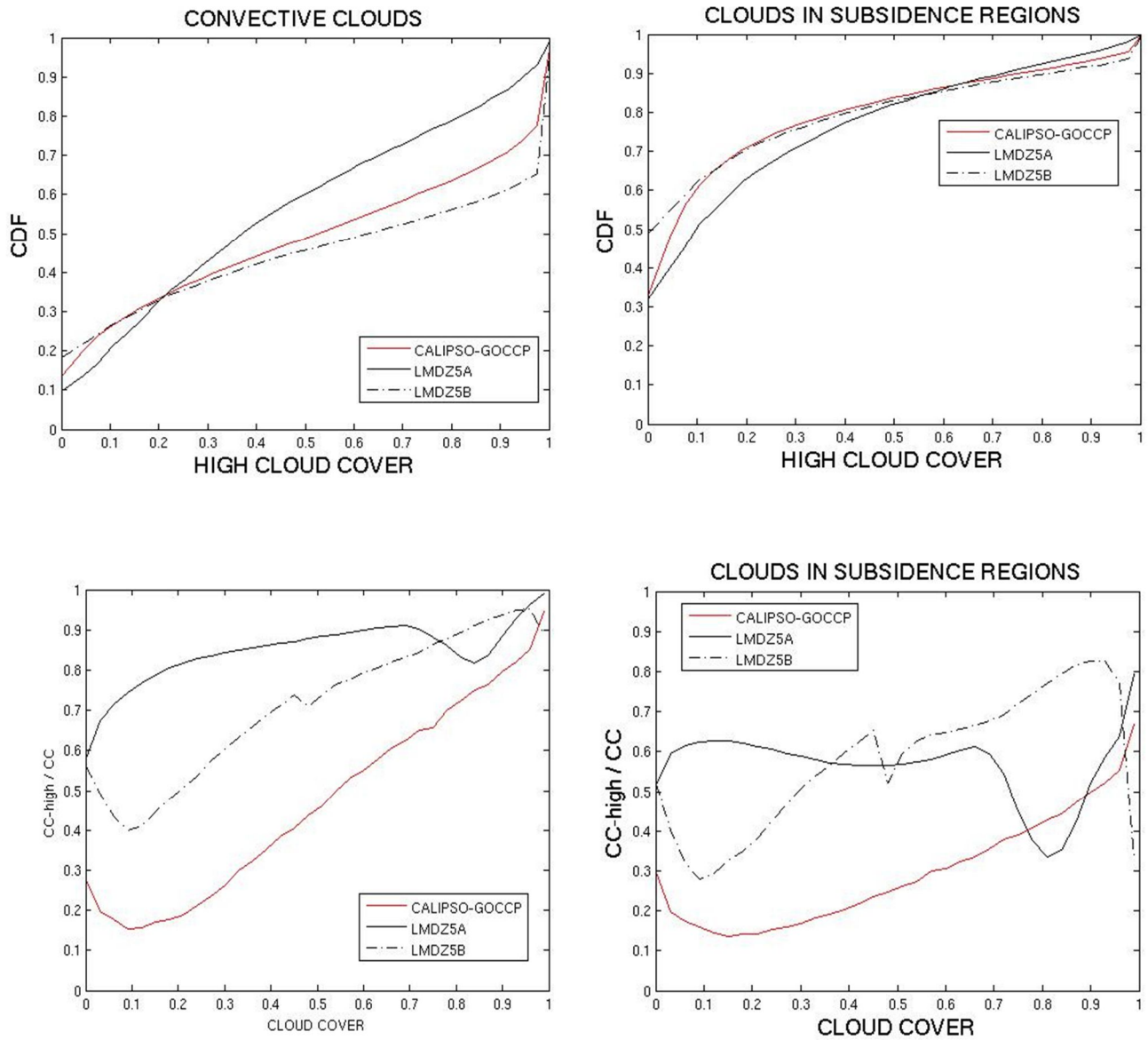
of points.



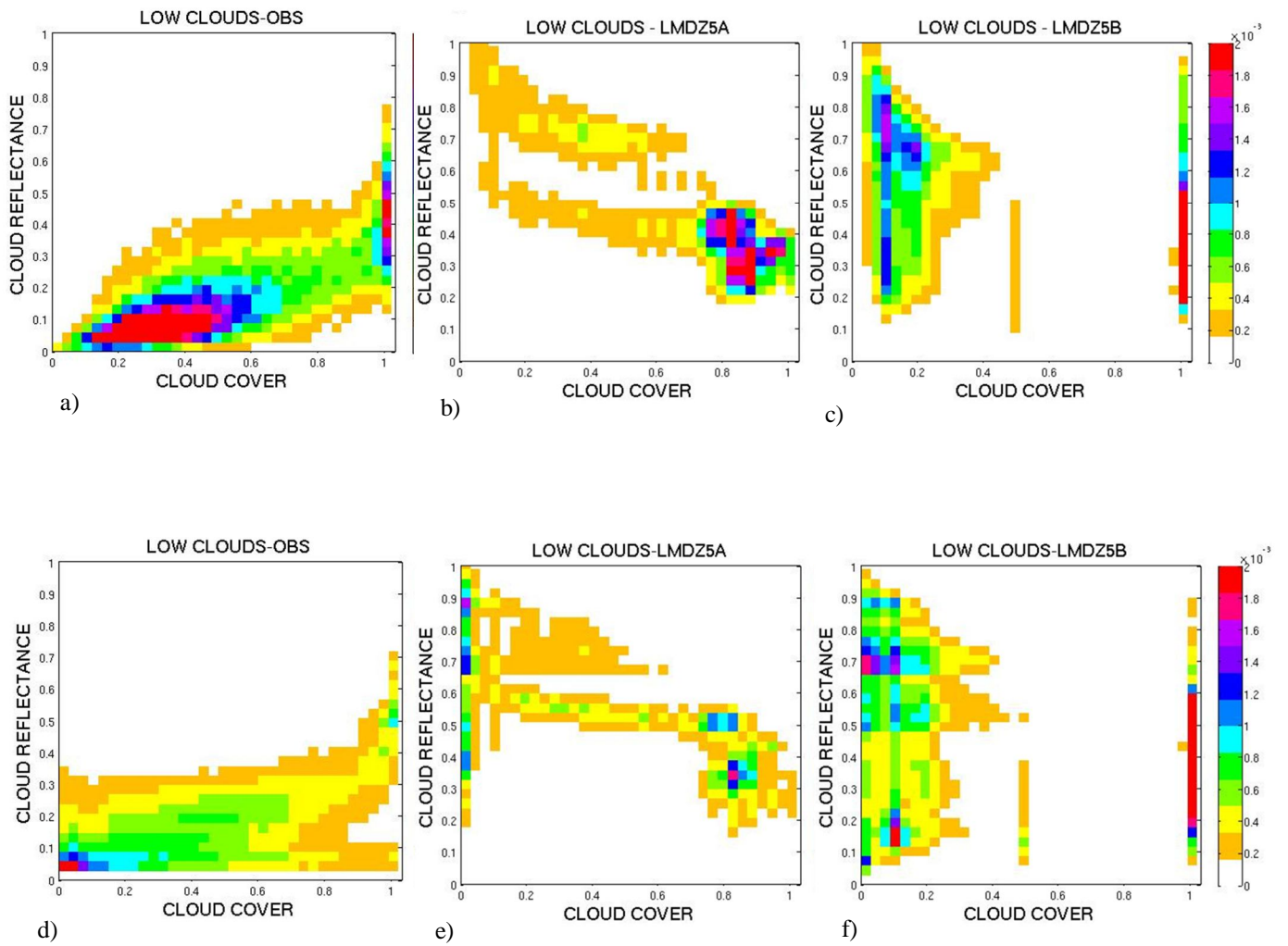
**Figure 4:** (a) PDF of cloud reflectances and (b,c,d) vertical profile of the cloud fraction CF3D for three classes defined by the grid average cloud reflectance (b)  $CR < 0.2$ , (c)  $0.2 < CR < 0.5$ , (d)  $CR > 0.5$ . Red line corresponds to observed values from PARASOL and CALIPSO-GOCCP respectively, black line corresponds to simulated values with LMDZ5A and the simulator and black dotted line corresponds to simulated values with LMDZ5B and the simulator. The data are instantaneous values and are taken only over the tropical oceans.



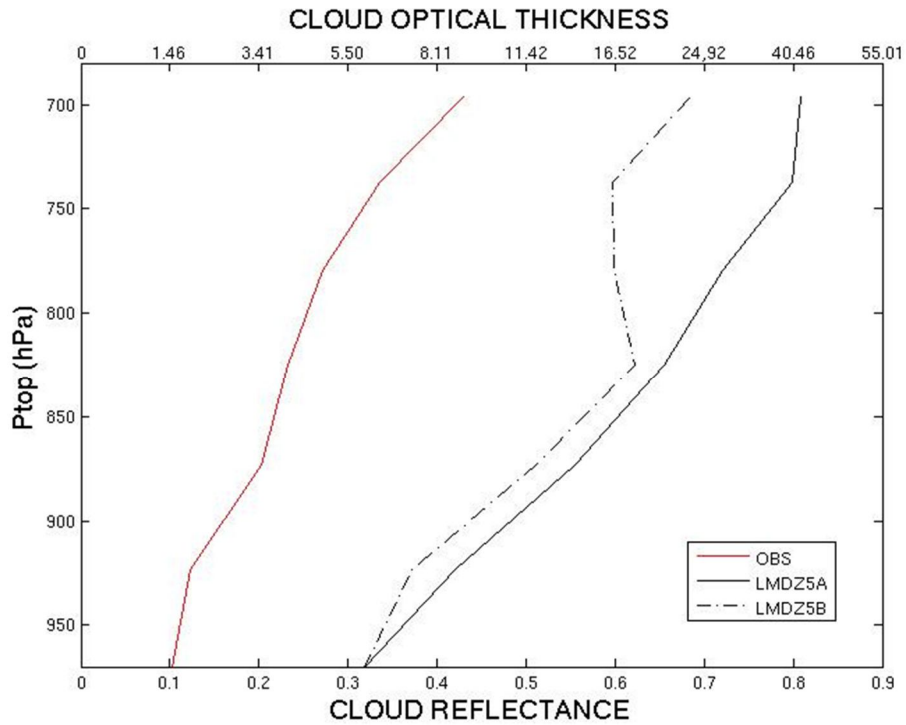
**Figure 5:** Cumulated distribution function of the cloud cover for high level clouds (upper row) and average relationship between total cloud cover and the normalized cloud cover of high level cloud (lower row, see text) in ascent (left column) and subsidence (right column) regions, observed with CALIPSO-GOCCP (red line), simulated with LMDZ5A and the simulator (black line), and simulated with LMDZ5B and the simulator (black dotted line). The cloud cover are instantaneous values and the ascent and subsidence regions are defined as regions over the tropical ocean where the monthly mean value of  $\omega_{500}$  is respectively negative and positive.



**Figure 6:** 2D histograms of instantaneous cloud reflectance and cloud cover over the tropical ocean for situations where low level clouds dominate ( $CC_{low} > 0.9 * CC$ ) (a, d) observed, (b, e) simulated with LMDZ5A and the simulator, and (c, f) simulated with LMDZ5B and the simulator. The upper line (a,b,c) corresponds to PARASOL observations, CALIPSO observations and simulator respectively and the lower line (d,e,f) corresponds to ISCCP. The color bar represents the number of points at each grid cell (cloud cover-cloud reflectance) divided by the total number of points.

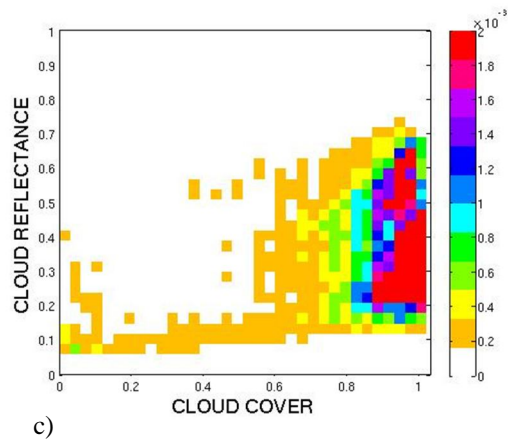
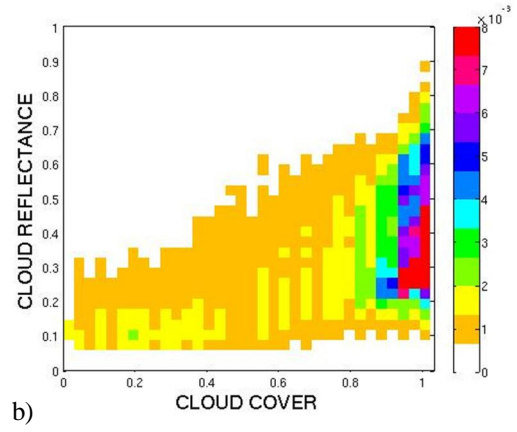
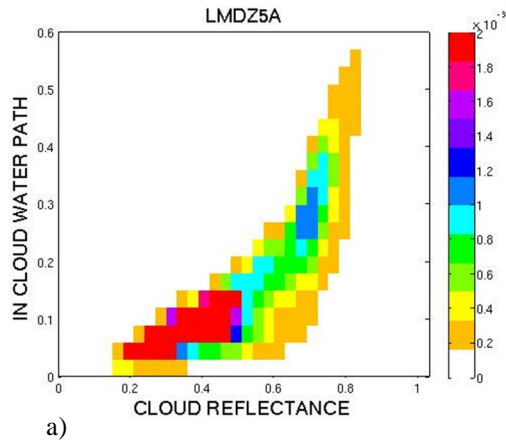


**Figure 7:** Instantaneous mean cloud reflectance as a function of cloud top pressure for mainly low-clouds situations (using the criterion:  $CC_{low} > 0.9 * CC$ ) over the tropical ocean, observed with PARASOL and CALIPSO-GOCCP (red line), simulated with LMDZ5A and the simulator (black line), and simulated with LMDZ5B and the simulator (black dotted line). CTP is defined as the highest level of low clouds where the local cloud cover is greater than 0.1.



**Figure 8:** 2D histograms of instantaneous of (a) cloud liquid water path versus cloud reflectance simulated with LMDZ5A for conditions where low-level-clouds dominate ( $CC_{low} > 0.9 * CC$ ) (b) cloud reflectance versus cloud cover with the modified parameterization in LMDZ5A (see text) for all clouds and (c) for conditions where low-level-clouds dominate

( $CC_{low} > 0.9 * CC$ ). The color bar represents the number of points at each grid cell divided by the total number of points.



872